Efficient Deployment Strategies for Network Localization with Assisting Nodes

Carlos A. Gómez-Vega, *Graduate Student Member, IEEE*, Zhenyu Liu, *Member, IEEE*, Carlos A. Gutiérrez, *Senior Member, IEEE*, Moe Z. Win, *Fellow, IEEE*, and Andrea Conti, *Fellow, IEEE*

Abstract—Location awareness is crucial for a variety of emerging applications. The accuracy of localization depends heavily on the spatial topology of the network, especially in complex and infrastructure-limited wireless environments. In these environments, assisting nodes can be deployed to achieve desirable performance. This paper presents efficient strategies for deploying assisting nodes to improve the localization accuracy of a target agent. Specifically, it provides a methodology to determine a finite set of candidate positions for the assisting nodes. Based on this methodology, we present a convex relaxation to select near-optimal positions for the assisting nodes and establish a theoretical limit on the localization accuracy provided by assisting nodes. We also propose an approximate dynamic programming algorithm to deploy assisting nodes with amenable complexity. A case study validates the proposed strategies and shows the benefits of deploying assisting nodes for accurate localization.

Index Terms—Localization, assisting nodes, node deployment, network operation, wireless networks

1 Introduction

Network localization [1] is a promising paradigm for providing ubiquitous position information of nodes in wireless networks [2], [3], [4], [5], [6], [7], [8], [9], [10], [11]. Such information is crucial for several applications in fifth generation (5G) and beyond ecosystems [12], [13], [14], including autonomy [15], [16], [17], [18], [19], crowd-sensing [20], [21], [22], [23], [24], [25], [26], smart cities [27], [28], [29], [30], [31], [32], [33], and Internet-of-Things [34], [35], [36], [37], [38]. The 3rd Generation Partnership Project (3GPP) has defined performance requirements for seven positioning service levels [13], [39], [40]. Location-aware networks must satisfy service-level requirements regardless of the operation conditions. However, meeting the required performance is challenging in complex wireless environments, especially if the network infrastructure is limited.

Location-aware networks consist of anchors with known positions and agents with unknown positions. The accuracy of localization depends on the wireless resources, propagation conditions, and nodes' deployment [41]. In particular, the exploitation of soft information [34] enables accurate localization in complex wireless environments, and its performance gain has been demonstrated in 5G and beyond ecosystems [12], [14], [42]. Furthermore, location-aware networks benefit from strategies for allocation of wireless resources [43], [44], [45] and coordination of nodes' transmissions [46], [47], [48]. Nonetheless, localization accuracy degrades in infrastructure-limited environments where the measurements and geometric relationships among nodes are inadequate for positioning. In these environments, *assisting nodes* [49] can be deployed to meet desirable performance (see Fig. 1). For example, the deployment of assisting nodes for public safety applications (e.g., via unmanned aerial vehicles (UAVs) [50], [51], [52] relying on spatial cooperation and heterogeneous measurements [53], [54], [55]) will enable reliable localization of victims and first responders in challenging environments [40, Section 5.4].

The deployment of wireless networks is mainly driven by communication demands [56], [57], [58], [59], [60], [61],

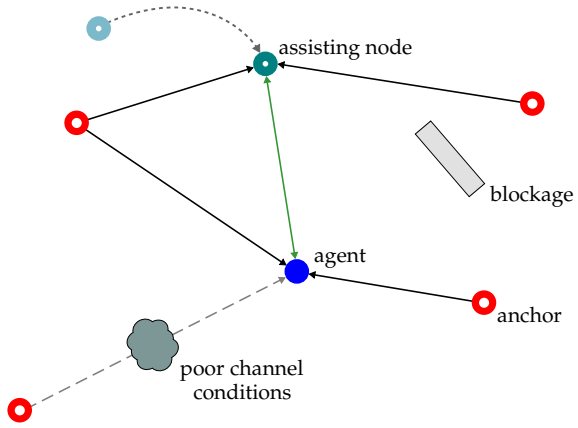

Fig. 1. Network localization with an assisting node. The agent receives insufficient position information from anchors due to the complex wireless environment and limited network infrastructure. The assisting node moves from an initial position (faded annulus) to an optimal position (bright annulus) determined by a node deployment strategy.

- *Carlos A. Gómez-Vega and Andrea Conti are with the Department of Engineering and CNIT, University of Ferrara, 44122 Ferrara, Italy. E-mail: cgomez@ieee.org, a.conti@ieee.org.*
- *Zhenyu Liu is with the Wireless Information and Network Sciences Laboratory, Massachusetts Institute of Technology, Cambridge, MA 02139 USA. E-mail: zliu14@mit.edu.*
- *Carlos A. Gutiérrez is with the Faculty of Science, Universidad Autónoma de San Luis Potosí, 78295 San Luis Potosí, Mexico. E-mail: cagutierrez@ieee.org.*
- *Moe Z. Win is with the Laboratory for Information and Decision Systems, Massachusetts Institute of Technology, Cambridge, MA 02139 USA. E-mail: moewin@mit.edu.*

The fundamental research described in this paper was supported, in part, by the Office of Naval Research under Grant N62909-22-1-2009, by the National Science Foundation under Grant CNS-2148251, and by funds from federal agency and industry partners in the RINGS program. The material in this paper was presented, in part, at the KICS Winter Conference, Pyeongchang, Korea, February 2021. (Corresponding author: Andrea Conti).

[62], [63], [64]. In particular, the role of the network topology in the position error has been studied in [65], [66], [67] and node deployment strategies for localization have been developed in [68], [69], [70], [71], [72], [73], [74]. The design of node deployment strategies relies on optimizing a performance metric expressed as a function of the nodes' positions. Localization performance metrics are defined in terms of the Fisher information matrix (FIM) [75], which describes the position information that agents obtain from measurements [76]. The structure and interpretation of the FIM (or equivalent forms such as the covariance matrix [77], [78]) can be exploited to design node deployment strategies under different optimality criteria [41].

Conventional node deployment strategies for localization focus on the anchor placement [69], [70], [71], [72], [73]. Such strategies are typically based on the assumption that anchors are placed on the boundary of a convex region containing the target agent and rely on standard optimization methods [79], [80]. While conventional node deployment strategies provide desirable anchor placements, new strategies to deploy possibly cooperative assisting nodes can enable efficient high-accuracy localization in complex wireless environments. In particular, the 3GPP has considered in-coverage, partial-coverage, and out-of-coverage use cases for localization in 5G and beyond ecosystems enabled by spatial cooperation among agents via sidelink communication [81], [82], [83], [84]. Hence, efficient network localization calls for general strategies to deploy assisting nodes considering knowledge from existing infrastructure, if any. The computational complexity of such strategies must be amenable to meet positioning latency requirements without compromising localization accuracy [12], [13].

The fundamental questions related to the deployment of assisting nodes are: (i) how does the localization accuracy of a target agent depend on the positions of assisting nodes; and (ii) how to determine optimal assisting node positions? The answers to these questions will provide guidelines for the deployment of assisting nodes. The goal of this paper is to develop node deployment strategies with amenable complexity to improve localization accuracy with assisting nodes. The key idea consists of determining a finite set of candidate positions to select near-optimal locations for the assisting nodes.

This paper presents near-optimal strategies to deploy assisting nodes for efficient network localization. Specifically, we introduce a methodology to determine a finite set of candidate positions and develop efficient strategies for deploying assisting nodes based on convex optimization and approximate dynamic programming (ADP). The key contributions of this paper are as follows:

- introduction of a methodology to determine candidate positions for the assisting nodes;
- development of efficient strategies for deploying assisting nodes; and
- quantification of the benefits provided by deploying assisting nodes for accurate localization.

The remaining sections are organized as follows: Section 2 formulates the node deployment problem. Section 3 provides the methodology to determine a finite set of candidate positions for the assisting nodes. Section 4 presents a convex relaxation to select near-optimal positions for the assisting nodes and establish a theoretical limit on the localization accuracy provided by assisting nodes. Section 5 develops an ADP algorithm for deploying assisting nodes with amenable complexity. Section 6 discusses the inverse node deployment problem of assisting nodes. Section 7 presents a case study. Finally, Section 8 gives our conclusions.

Notations: Random variables are displayed in sans serif, upright fonts; their realizations in serif, italic fonts. Vectors and matrices are denoted by bold lowercase and uppercase letters, respectively. For example, a variable is denoted by x; a random vector and its realization are denoted by $\mathbf{x}$ and $\boldsymbol{x}$, respectively; a matrix is denoted by $\boldsymbol{X}$. Sets are denoted by calligraphic font. For example, a set is denoted by $\mathcal{X}$. The m-dimensional vector of zeros (resp. ones) is denoted by $\mathbf{0}_m$ (resp. $\mathbf{1}_m$): the subscript is removed when the dimension of the vector is clear from the context. For a vector $\boldsymbol{x}$ and a matrix $\boldsymbol{X}$, the transpose is denoted by $\boldsymbol{x}^{\mathrm{T}}$ and $\boldsymbol{X}^{\mathrm{T}}$, respectively. The trace and determinant of a matrix $\boldsymbol{X}$ are denoted by $\mathrm{tr}\{\boldsymbol{X}\}$ and $\det\{\boldsymbol{X}\}$, respectively. The Euclidean norm and direction of a vector $\boldsymbol{x}$ are denoted by $\|\boldsymbol{x}\|$ and $\angle\boldsymbol{x}$, respectively. The inequalities $\boldsymbol{a} \preccurlyeq \boldsymbol{b}$ and $\boldsymbol{a} \succcurlyeq \boldsymbol{b}$ denote element-wise inequalities between vectors $\boldsymbol{a}$ and $\boldsymbol{b}$. Notation $\mathrm{diag}\{\cdot\}$ represents a diagonal matrix with the arguments being its diagonal elements.

2 Problem Formulation

This section presents the system model, describes the localization performance metrics, and formulates the node deployment problem of assisting nodes.

2.1 System Model

Consider a location-aware network with a target agent and N_{b} anchors. The goal is to improve the localization accuracy of the target agent by deploying N_{c} assisting nodes (see Fig. 2). The assisting nodes may be subject to position uncertainty and perform measurements with the target agent and neighboring anchors. The index sets of anchors and assisting nodes are $\mathcal{N}_{\mathrm{b}} = \{1, 2, \ldots, N_{\mathrm{b}}\}$ and $\mathcal{N}_{\mathrm{c}} = \{N_{\mathrm{b}}+1, N_{\mathrm{b}}+2, \ldots, N_{\mathrm{b}}+N_{\mathrm{c}}\}$, respectively. The target agent is indexed as the node zero. The position of node i is denoted by $\boldsymbol{p}_i \in \mathbb{R}^2$. The distance and angle between the positions of nodes i and j are denoted by $d_{i,j} = \|\boldsymbol{p}_i - \boldsymbol{p}_j\|$ and $\phi_{i,j} = \angle(\boldsymbol{p}_i - \boldsymbol{p}_j)$, respectively. The node deployment strategy aims to determine the assisting node positions, $\boldsymbol{p}_{\mathrm{c}} = [\boldsymbol{p}_{N_{\mathrm{b}}+1}^{\mathrm{T}}, \boldsymbol{p}_{N_{\mathrm{b}}+2}^{\mathrm{T}}, \ldots, \boldsymbol{p}_{N_{\mathrm{b}}+N_{\mathrm{c}}}^{\mathrm{T}}]^{\mathrm{T}}$, that maximally improve the localization accuracy of the target agent. The positions of assisting nodes are restricted by K disjoint deployment regions, $\mathcal{R}_1, \mathcal{R}_2, \ldots, \mathcal{R}_K$, enumerated in counterclockwise direction. The set of possible assisting node positions is denoted by $\mathcal{S} = \cup_{k=1}^{K} \mathcal{R}_k$. This set excludes all the positions where assisting nodes cannot be deployed due to delimitation or blockages given map information and knowledge of the line-of-sight (LOS) and non-line-of-sight (NLOS) conditions in the environment.

Let $\boldsymbol{J}(\boldsymbol{p}_0, \boldsymbol{p}_{\mathrm{c}})$ denote the equivalent Fisher information matrix (EFIM) [76] for the positions of the target agent and assisting nodes, given by (1) shown at the bottom of next page. In (1), the matrix $\boldsymbol{J}_{\mathrm{e}}^{\mathrm{A}}(\boldsymbol{p}_i)$ represents the position information that node i obtains from anchors; and the matrix $\boldsymbol{C}_{i,j}$

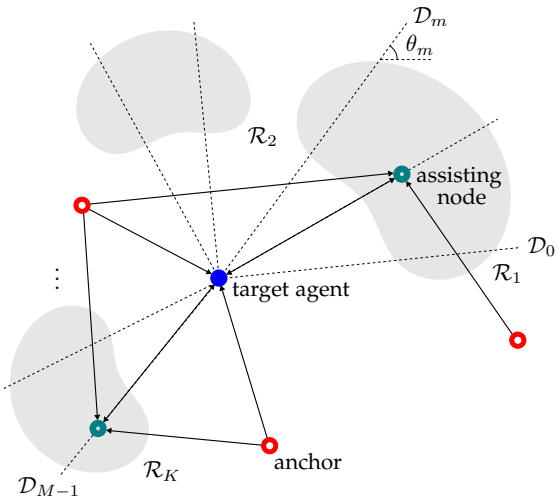

Fig. 2. Node deployment scenario: assisting nodes are deployed to improve the localization accuracy of a target agent. The positions of assisting nodes are restricted by K deployment regions (gray areas).

represents the position information that node i obtains from spatial cooperation with node j. Such matrices are given, respectively, by

$$\boldsymbol{J}_{\mathrm{e}}^{\mathrm{A}}(\boldsymbol{p}_i) = \sum_{j\in\mathcal{N}_{\mathrm{b}}} \lambda_{i,j}\, \boldsymbol{J}_{\mathrm{r}}(\phi_{i,j}) \tag{2a}$$

$$\boldsymbol{C}_{i,j} = \boldsymbol{C}_{j,i} = (\lambda_{i,j} + \lambda_{j,i})\, \boldsymbol{J}_{\mathrm{r}}(\phi_{i,j}) \tag{2b}$$

where $\lambda_{i,j}$ is referred to as the range information intensity (RII) between nodes i and j; and $\boldsymbol{J}_{\mathrm{r}}(\phi)$ is referred to as the range direction matrix (RDM) with angle ϕ [76].

The RII and RDM depend on the deployment of nodes i and j, and are given by

$$\lambda_{i,j} = \Lambda(d_{i,j}) = \frac{8\pi^2\beta^2}{c^2}\,(1-\chi_{i,j})\,\gamma_{i,j}(d_{i,j}) \tag{3a}$$

$$\boldsymbol{J}_{\mathrm{r}}(\phi) = \begin{bmatrix} \cos^2(\phi) & \cos(\phi)\sin(\phi) \\ \cos(\phi)\sin(\phi) & \sin^2(\phi) \end{bmatrix} \tag{3b}$$

respectively. In (3a), the RII is expressed as a function of distance $d_{i,j}$ in which β and c are the effective bandwidth and propagation speed of the transmitted signal, respectively; $\chi_{i,j} \in [0,1)$ is a realization of the path-overlap coefficient (POC) describing the degradation of the RII due to multipath propagation from node j to node i;[1] and $\gamma_{i,j}(d_{i,j})$ is the signal-to-noise ratio (SNR) of the first path received from node j at node i as a function of $d_{i,j}$. The SNR of the first path received from node j at node i is given by

$$\gamma_{i,j}(d_{i,j}) = G\frac{P_j}{d_{i,j}^{\alpha} N_0} \tag{4}$$

where P_j is the transmitting power level of node j, $\alpha \geqslant 0$ is the path-loss exponent, N_0 is the one-sided power spectral density of the noise component, and G is a gain that depends on the center frequency and antenna directivity. We consider that the target agent and assisting nodes have transmitting power P_{c}.[2]

To design strategies for deploying assisting nodes, consider the position information of the target agent. From (1), the 2×2 EFIM for the position of the target agent as a function of the assisting node positions is given by

$$\boldsymbol{J}_{\mathrm{e}}(\boldsymbol{p}_{\mathrm{c}};\boldsymbol{p}_0) = \boldsymbol{J}_{\mathrm{e}}^{\mathrm{A}}(\boldsymbol{p}_0) + \sum_{j\in\mathcal{N}_{\mathrm{c}}} \xi_{0,j}\boldsymbol{J}_{\mathrm{r}}(\phi_{0,j}) \tag{5}$$

where $\xi_{0,j} = \varsigma(d_{0,j},\phi_{0,j})$ denotes the equivalent ranging coefficient (ERC) obtained from spatial cooperation between the target agent and the assisting node j. The ERC is given by

$$\varsigma(d_{0,j},\phi_{0,j}) = \frac{r_{0,j}}{1+r_{0,j}\Delta_{0,j}} \tag{6}$$

where $r_{0,j} = \lambda_{0,j} + \lambda_{j,0}$ depends on the deployment of the target agent and assisting node j according to (3a), and

$$\Delta_{0,j} = \mathrm{tr}\Big\{\boldsymbol{J}_{\mathrm{r}}(\phi_{0,j})\big[\boldsymbol{J}_{\mathrm{e}}^{\mathrm{A}}(\boldsymbol{p}_j)\big]^{-1}\Big\}. \tag{7}$$

The term $\Delta_{0,j}$ penalizes the ERC from spatial cooperation with assisting node j due to its position uncertainty, and, as a special case, $\Delta_{0,j} = 0$ if it has perfect knowledge of its own position. In this special case, the assisting node j may be viewed as an assisting anchor with $r_{0,j} = \lambda_{0,j}$.[3]

2.2 Localization Performance Metrics

The localization accuracy of the target agent can be quantified by the mean-square error (MSE) of its position estimator. Let $\hat{\mathbf{p}}_0$ denote an unbiased estimator of $\boldsymbol{p}_0$ based on the noisy measurements that the target agent obtains from anchors and assisting nodes. From the information inequality, the MSE of the position estimator $\hat{\mathbf{p}}_0$ is lower bounded by the squared position error bound (SPEB) [76], which is given as

$$\mathcal{P}(\boldsymbol{p}_{\mathrm{c}};\boldsymbol{p}_0) = \mathrm{tr}\Big\{\big[\boldsymbol{J}_{\mathrm{e}}(\boldsymbol{p}_{\mathrm{c}};\boldsymbol{p}_0)\big]^{-1}\Big\}. \tag{8}$$

1. The POC depends on the inter-arrival delays of the multipath components in the first contiguous cluster of the received signal [76].

2. The transmitting power of cooperative nodes (e.g., target agent and assisting nodes) is smaller than that of anchors.

3. Even though the problem formulation includes this special case, the assumption of assisting nodes without position uncertainty may not be valid in most practical systems.

$$\boldsymbol{J}(\boldsymbol{p}_0,\boldsymbol{p}_{\mathrm{c}}) = \begin{bmatrix} \boldsymbol{J}_{\mathrm{e}}^{\mathrm{A}}(\boldsymbol{p}_0) + \sum\limits_{j\in\mathcal{N}_{\mathrm{c}}} \boldsymbol{C}_{0,j} & -\boldsymbol{C}_{0,N_{\mathrm{b}}+1} & -\boldsymbol{C}_{0,N_{\mathrm{b}}+2} & \cdots & -\boldsymbol{C}_{0,N_{\mathrm{b}}+N_{\mathrm{c}}} \\ -\boldsymbol{C}_{N_{\mathrm{b}}+1,0} & \boldsymbol{J}_{\mathrm{e}}^{\mathrm{A}}(\boldsymbol{p}_{N_{\mathrm{b}}+1}) + \boldsymbol{C}_{N_{\mathrm{b}}+1,0} & \mathbf{0} & \cdots & \mathbf{0} \\ -\boldsymbol{C}_{N_{\mathrm{b}}+2,0} & \mathbf{0} & \boldsymbol{J}_{\mathrm{e}}^{\mathrm{A}}(\boldsymbol{p}_{N_{\mathrm{b}}+2}) + \boldsymbol{C}_{N_{\mathrm{b}}+2,0} & \cdots & \mathbf{0} \\ \vdots & \vdots & \vdots & \ddots & \vdots \\ -\boldsymbol{C}_{N_{\mathrm{b}}+N_{\mathrm{c}},0} & \mathbf{0} & \mathbf{0} & \cdots & \boldsymbol{J}_{\mathrm{e}}^{\mathrm{A}}(\boldsymbol{p}_{N_{\mathrm{b}}+N_{\mathrm{c}}}) + \boldsymbol{C}_{N_{\mathrm{b}}+N_{\mathrm{c}},0} \end{bmatrix} \tag{1}$$

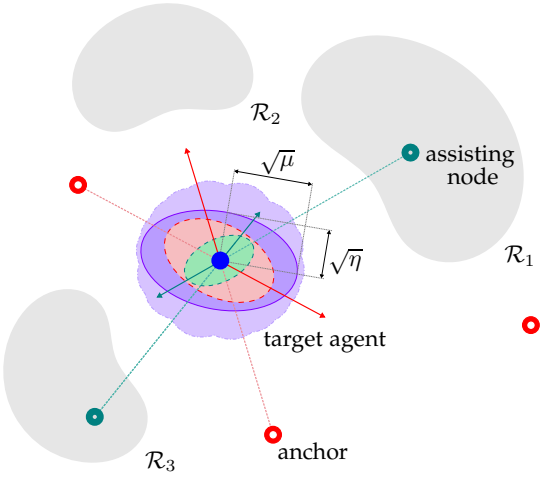

Fig. 3. Geometric interpretation of the EFIM for the position of a target agent. Arrows denote the direction of inter-node measurements, and the length of an arrow represents the amount of wireless resources employed. The red ellipse represents the position information obtained from anchors; the green ellipse represents the position information obtained from spatial cooperation with assisting nodes; and the purple ellipse represents the position information obtained from anchors and spatial cooperation with assisting nodes. The purple shade represents the area where the information ellipse can exist given the possible assisting node positions.

This lower bound is asymptotically achievable by maximum likelihood estimators in high SNR regimes and can be adopted as the localization performance metric for the design of node deployment strategies [41]. Furthermore, a measure of the confidence of $\hat{\mathbf{p}}_0$ based on the geometric interpretation of the EFIM as an information ellipse can also be employed as localization performance metric [76].

Consider the eigenvalue decomposition of the 2×2 EFIM for the position of the target agent given by

$$\boldsymbol{J}_{\mathrm{e}}(\boldsymbol{p}_{\mathrm{c}};\boldsymbol{p}_0) = \boldsymbol{U}_{\vartheta}\begin{bmatrix}\mu & 0\\ 0 & \eta\end{bmatrix}\boldsymbol{U}_{\vartheta}^{\mathrm{T}} \tag{9}$$

where μ and η are the eigenvalues of $\boldsymbol{J}_{\mathrm{e}}(\boldsymbol{p}_{\mathrm{c}};\boldsymbol{p}_0)$ and $\boldsymbol{U}_{\vartheta}$ is a rotation matrix [76]. From (9), the SPEB of the target agent can be expressed as

$$\mathcal{P}(\boldsymbol{p}_{\mathrm{c}};\boldsymbol{p}_0) = \mathrm{tr}\left\{\begin{bmatrix}\mu & 0\\ 0 & \eta\end{bmatrix}^{-1}\right\} = \mu^{-1}+\eta^{-1}\,. \tag{10}$$

The information ellipse of a 2×2 EFIM $\boldsymbol{J}_{\mathrm{e}}(\boldsymbol{p}_{\mathrm{c}};\boldsymbol{p}_0)$ is defined as the set of points [76]

$$\left\{\boldsymbol{w}\in\mathbb{R}^2 :\ \boldsymbol{w}^{\mathrm{T}}[\boldsymbol{J}_{\mathrm{e}}(\boldsymbol{p}_{\mathrm{c}};\boldsymbol{p}_0)]^{-1}\boldsymbol{w}=1\right\}. \tag{11}$$

Fig. 3 illustrates the geometric interpretation of the EFIM for the position of a target agent as an information ellipse with major and minor axes equal to $\sqrt{\mu}$ and $\sqrt{\eta}$, respectively. This ellipse represents the position information obtained by the target agent from anchors and spatial cooperation with assisting nodes.

The area of the information ellipse can be used as a measure of the confidence of $\hat{\mathbf{p}}_0$. In particular, a large information ellipse is desirable for accurate localization. Nevertheless, the largest information ellipse does not necessarily provide the lowest SPEB [76]. Since the area of the information ellipse is related to the determinant of the EFIM, we consider the alternative performance metric given by

$$\mathcal{Q}(\boldsymbol{p}_{\mathrm{c}};\boldsymbol{p}_0) = \det\{\boldsymbol{J}_{\mathrm{e}}(\boldsymbol{p}_{\mathrm{c}};\boldsymbol{p}_0)\}\,. \tag{12}$$

2.3 Node Deployment Problem of Assisting Nodes

The goal of the node deployment strategy is to determine the positions where assisting nodes should be placed to maximally improve the localization accuracy of a target agent. Since the possible assisting node positions are described by the set $\mathcal{S}$, the node deployment problem can be formulated as

$$\begin{aligned}\mathscr{P}\colon\ &\underset{\boldsymbol{p}_{\mathrm{c}}}{\text{minimize}} \quad \mathcal{P}(\boldsymbol{p}_{\mathrm{c}};\boldsymbol{p}_0)\\ &\text{subject to}\ \ \boldsymbol{p}_i\in\mathcal{S},\quad i\in\mathcal{N}_{\mathrm{c}}\,.\end{aligned}$$

Alternatively, the problem can be formulated by considering $\mathcal{Q}(\boldsymbol{p}_{\mathrm{c}};\boldsymbol{p}_0)$ with the goal of maximizing the confidence of the position estimator $\hat{\mathbf{p}}_0$ rather than minimizing the SPEB directly. In this case, problem $\mathscr{P}$ would be formulated by replacing the objective function with $-\mathcal{Q}(\boldsymbol{p}_{\mathrm{c}};\boldsymbol{p}_0)$.

Solving $\mathscr{P}$ is difficult because its objective function is, in general, not convex with $\boldsymbol{p}_{\mathrm{c}}$ due to symmetrical patterns caused by permutations of the positions and because $\mathcal{S}$ can describe complicated problem instantiations.[4] Moreover, the solutions to $\mathscr{P}$ can describe clusters of assisting nodes, i.e., assisting nodes deployed in close proximity to each other. To provide a more tractable solution to this problem, we consider a finite set of candidate positions from which the node deployment strategy selects near-optimal locations for the assisting nodes. The following section will introduce a methodology to determine a finite set of candidate positions for the assisting nodes.

3 Discretization of Deployment Regions

Consider the polar coordinates of the assisting node positions relative to the position of the target agent $\boldsymbol{p}_0$ as reference point. Let $\boldsymbol{d} = [\,d_{0,N_{\mathrm{b}}+1}, d_{0,N_{\mathrm{b}}+2},\ldots,d_{0,N_{\mathrm{b}}+N_{\mathrm{c}}}]^{\mathrm{T}}$ and $\boldsymbol{\phi} = [\,\phi_{0,N_{\mathrm{b}}+1}, \phi_{0,N_{\mathrm{b}}+2},\ldots,\phi_{0,N_{\mathrm{b}}+N_{\mathrm{c}}}]^{\mathrm{T}}$ denote the vectors of distance and angle components of the polar coordinates of the assisting nodes with respect to $\boldsymbol{p}_0$, respectively. Moreover, consider the function $\boldsymbol{g}(d,\phi) = \boldsymbol{p}_0 + d\,[\cos(\phi),\sin(\phi)]^{\mathrm{T}}$ to obtain the Cartesian coordinates of the position represented by the polar coordinates (d,ϕ). The EFIM for the position of the target agent can be rewritten in terms of $\boldsymbol{d}$ and $\boldsymbol{\phi}$ as

$$\boldsymbol{J}_{\mathrm{e}}(\boldsymbol{d},\boldsymbol{\phi};\boldsymbol{p}_0) = \boldsymbol{J}_{\mathrm{e}}^{\mathrm{A}}(\boldsymbol{p}_0) + \sum_{j\in\mathcal{N}_{\mathrm{c}}}\varsigma(d_{0,j},\phi_{0,j})\,\boldsymbol{J}_{\mathrm{r}}(\phi_{0,j}) \tag{13}$$

in which $\boldsymbol{p}_j = \boldsymbol{g}(d_{0,j},\phi_{0,j})$ for $j\in\mathcal{N}_{\mathrm{c}}$.

The optimization of a performance metric equivalent to (8) based on $\boldsymbol{J}_{\mathrm{e}}(\boldsymbol{d},\boldsymbol{\phi};\boldsymbol{p}_0)$ can be performed by first establishing the distance components for a given set of angles and then determining the appropriate angles [41]. The distance component for a fixed angle $\phi_{0,j}$ is given by

$$d_{0,j}^{*} = \underset{\{d_{0,j}:\,\boldsymbol{g}(d_{0,j},\phi_{0,j})\in\mathcal{S}\}}{\arg\max}\ \varsigma(d_{0,j},\phi_{0,j})\,. \tag{14}$$

4. The optimization of non-convex functions is challenging due to the existence of locally optimal solutions that are not globally optimal [80].

This problem can be solved by one-dimensional optimization methods since the objective function only depends on a single variable. Note that $\varsigma(d_{0,j},\phi_{0,j})$ also depends on the propagation conditions that an assisting node will experience if it is deployed at the position described by $\boldsymbol{g}(d_{0,j},\phi_{0,j})\in\mathcal{S}$. We consider that the POCs describing the propagation conditions for such positions are known.[5]

The next step consists of optimizing the angle components given the corresponding distances. This step is difficult because the possible angles are described by disjoint intervals and the objective function is not convex with ϕ. Hence, we consider that the angles $\phi_{0,j}$ belong to a finite set of M possible directions $\Theta=\{\theta_0,\theta_1,\ldots,\theta_{M-1}\}$. The discretization of the angles describes a reduced version of the set $\mathcal{S}$. The reduced set of possible assisting node positions is denoted by $\check{\mathcal{S}}=\cup_{m=0}^{M-1}(\mathcal{D}_m\cap\mathcal{S})$, where $\mathcal{D}_m=\{\boldsymbol{z}\in\mathbb{R}^2:\angle(\boldsymbol{z}-\boldsymbol{p}_0)=\theta_m\}$ is the set of positions described by the angle θ_m with respect to $\boldsymbol{p}_0$ (see Fig. 2).

A discretization method to determine the angles θ_m is described next. Let θ_k^{L} and θ_k^{U} denote the lower and upper angle constraints of the deployment region k with respect to $\boldsymbol{p}_0$ as reference point. Moreover, let $a_k=\theta_k^{\mathrm{U}}-\theta_k^{\mathrm{L}}$ denote the length of the interval of angles over which assisting nodes can be placed in the deployment region k, which is referred to as the aperture of the deployment region k. The apertures of the deployment regions are concatenated and considered as a single interval with total aperture $A=\sum_{k=1}^{K}a_k$. Then, the set of angles $\{\check{\theta}_0,\check{\theta}_1,\ldots,\check{\theta}_{M-1}\}$ is obtained with $\check{\theta}_m$ given by

$$\check{\theta}_m=(m+1)\frac{A}{M+1}\,. \tag{15}$$

To determine the possible angles θ_m, the values $\check{\theta}_m$ are mapped to the intervals described by the deployment regions. This mapping is given by

$$h(\check{\theta}_m)=\begin{cases}\check{\theta}_m+\theta_1^{\mathrm{L}} & \text{if} \quad 0<\check{\theta}_m\leqslant a_1\\ \check{\theta}_m+\theta_2^{\mathrm{L}}-a_1 & \text{if} \quad a_1<\check{\theta}_m\leqslant a_1+a_2\\ \qquad\vdots & \\ \check{\theta}_m+\theta_K^{\mathrm{L}}-\sum_{k=1}^{K-1}a_k & \text{if} \quad \sum_{k=1}^{K-1}a_k<\check{\theta}_m\leqslant\sum_{k=1}^{K}a_k\,.\end{cases} \tag{16}$$

The angle discretization enables establishing a finite set of possible assisting node positions. The positions in this set are referred to as candidate positions since the node deployment strategy will select the locations of assisting nodes among them. Specifically, each possible angle θ_m is paired with a distance d_m, which, from (14), is given by

$$d_m=\underset{\{d:\,\boldsymbol{g}(d,\theta_m)\in\check{\mathcal{S}}\}}{\arg\max}\ \varsigma(d,\theta_m)\,. \tag{17}$$

The polar coordinates (d_m,θ_m) determine the candidate position $\check{\boldsymbol{p}}_m=\boldsymbol{g}(d_m,\theta_m)$. An assisting node deployed at $\check{\boldsymbol{p}}_m$ will provide position information to the target agent with ERC $\check{\xi}_m=\varsigma(d_m,\theta_m)$. The vectors of candidate positions and ERCs are denoted by $\check{\boldsymbol{p}}_{\mathrm{c}}=[\check{\boldsymbol{p}}_0^{\mathrm{T}},\check{\boldsymbol{p}}_1^{\mathrm{T}},\ldots,\check{\boldsymbol{p}}_{M-1}^{\mathrm{T}}]^{\mathrm{T}}$ and $\check{\boldsymbol{\xi}}_{\mathrm{c}}=[\check{\xi}_0,\check{\xi}_1,\ldots,\check{\xi}_{M-1}]^{\mathrm{T}}$, respectively. Algorithm 1 describes the steps to discretize the deployment regions and establish a finite set of candidate positions.

5. Realizations of the POCs can be obtained by generating the received waveform or by means of a statistical model [85].

Algorithm 1 Discretization of Deployment Regions

Input: Target agent position $\boldsymbol{p}_0$, deployment regions $\mathcal{R}_1,\mathcal{R}_2,\ldots,\mathcal{R}_K$, and number of candidate positions M.
Output: Candidate positions $\check{\boldsymbol{p}}_{\mathrm{c}}$ and ERCs $\check{\boldsymbol{\xi}}_{\mathrm{c}}$.

for $k=1$ to K **do**
  Determine the angle constraints θ_k^{L} and θ_k^{U}.
  $a_k\leftarrow\theta_k^{\mathrm{U}}-\theta_k^{\mathrm{L}}$.
end for
$A\leftarrow\sum_{k=1}^{K}a_k$.
for $m=0$ to $M-1$ **do**
  $\check{\theta}_m\leftarrow(m+1)\,[A/(M+1)]$.
  $\theta_m\leftarrow h(\check{\theta}_m)$.
  $d_m\leftarrow\underset{\{d:\,\boldsymbol{g}(d,\theta_m)\in\check{\mathcal{S}}\}}{\arg\max}\ \varsigma(d,\theta_m)$.
  $\check{\boldsymbol{p}}_m\leftarrow\boldsymbol{g}(d_m,\theta_m)$.
  $\check{\xi}_m\leftarrow\varsigma(d_m,\theta_m)$.
end for
$\check{\boldsymbol{p}}_{\mathrm{c}}\leftarrow[\check{\boldsymbol{p}}_0^{\mathrm{T}},\check{\boldsymbol{p}}_1^{\mathrm{T}},\ldots,\check{\boldsymbol{p}}_{M-1}^{\mathrm{T}}]^{\mathrm{T}}$.
$\check{\boldsymbol{\xi}}_{\mathrm{c}}\leftarrow[\check{\xi}_0,\check{\xi}_1,\ldots,\check{\xi}_{M-1}]^{\mathrm{T}}$.

By considering the finite set of candidate positions $\{\check{\boldsymbol{p}}_0,\check{\boldsymbol{p}}_1,\ldots,\check{\boldsymbol{p}}_{M-1}\}$, the EFIM for the position of the target agent can be rewritten as

$$\check{\boldsymbol{J}}_{\mathrm{e}}(\boldsymbol{u};\boldsymbol{p}_0)=\boldsymbol{J}_{\mathrm{e}}^{\mathrm{A}}(\boldsymbol{p}_0)+\sum_{m=0}^{M-1}u_m\check{\xi}_m\boldsymbol{J}_{\mathrm{r}}(\theta_m) \tag{18}$$

where $\boldsymbol{u}=[u_0,u_1,\ldots,u_{M-1}]^{\mathrm{T}}$ with $u_m\in\{0,1\}$ encoding whether an assisting node is deployed ($u_m=1$) at the position $\check{\boldsymbol{p}}_m$ or not ($u_m=0$). Then, the performance metrics introduced in Section 2.2 can be rewritten as

$$\check{\mathcal{P}}(\boldsymbol{u};\boldsymbol{p}_0)=\mathrm{tr}\Big\{\big[\check{\boldsymbol{J}}_{\mathrm{e}}(\boldsymbol{u};\boldsymbol{p}_0)\big]^{-1}\Big\} \tag{19a}$$

$$\check{\mathcal{Q}}(\boldsymbol{u};\boldsymbol{p}_0)=\det\big\{\check{\boldsymbol{J}}_{\mathrm{e}}(\boldsymbol{u};\boldsymbol{p}_0)\big\} \tag{19b}$$

which are the counterparts of (8) and (12), respectively, considering the EFIM for the position of the target agent as a function of $\boldsymbol{u}$. The node deployment strategy based on (19a) (or (19b)) aims to select the N_{c} positions where assisting nodes should be deployed to maximally improve the localization accuracy of the target agent. This is expressed by the problem

$$\mathscr{P}_{\mathrm{s}}\colon\ \underset{\boldsymbol{u}}{\text{minimize}}\quad\check{\mathcal{P}}(\boldsymbol{u};\boldsymbol{p}_0) \tag{20a}$$

$$\text{subject to}\quad\mathbf{1}^{\mathrm{T}}\boldsymbol{u}=N_{\mathrm{c}} \tag{20b}$$

$$u_m\in\{0,1\},\quad m=0,1,\ldots,M-1 \tag{20c}$$

where $\mathscr{P}_{\mathrm{s}}$ denotes the formulation of the node deployment task as a selection problem [77]. In $\mathscr{P}_{\mathrm{s}}$, (20b) represents the constraint on the total number of available assisting nodes for deployment, i.e., $\sum_{m=0}^{M-1}u_m=N_{\mathrm{c}}$, and (20c) represents the Boolean constraints for the selection variables. Hence, the optimization problem requires $M\geqslant N_{\mathrm{c}}$ candidate positions. Note that the assisting node positions $\boldsymbol{p}_{\mathrm{c}}$ correspond to the candidate positions $\check{\boldsymbol{p}}_m$ with $u_m=1$.

The selection problem $\mathscr{P}_{\mathrm{s}}$ may be viewed as a relaxation of $\mathscr{P}$ since it considers a finite subset of possible assisting node positions. Nonetheless, approximate solutions to the node deployment problem of assisting nodes (which is

generally difficult to solve in its conventional form $\mathscr{P}$) can be obtained by considering the form of $\mathscr{P}_{\mathrm{s}}$. Note that the choice of the parameter M involves a tradeoff between the accuracy of the approximation and the complexity of solving $\mathscr{P}_{\mathrm{s}}$. Furthermore, the problem can also be formulated by employing $-\check{\mathcal{Q}}(\boldsymbol{u};\boldsymbol{p}_0)$ as objective function with the goal of maximizing the confidence of the position estimator.

4 Convex Relaxation

The objective function $\check{\mathcal{P}}(\boldsymbol{u};\boldsymbol{p}_0)$ in (20a) is convex for $\boldsymbol{u} \succcurlyeq \boldsymbol{0}$ [41]. This allows to obtain a convex relaxation of the combinatorial problem $\mathscr{P}_{\mathrm{s}}$ by replacing the Boolean constraints in (20c) with the box constraints $0 \leqslant u_m \leqslant 1$. Let $\mathscr{P}_{\mathrm{sc}}$ denote the convex relaxation of $\mathscr{P}_{\mathrm{s}}$ expressed as

$$\begin{aligned}\mathscr{P}_{\mathrm{sc}}\colon \ \underset{\boldsymbol{u}}{\text{minimize}} \quad & \check{\mathcal{P}}(\boldsymbol{u};\boldsymbol{p}_0) \\ \text{subject to} \quad & \mathbf{1}^{\mathrm{T}}\boldsymbol{u} = N_{\mathrm{c}} \\ & 0 \leqslant u_m \leqslant 1, \quad m = 0,1,\ldots,M-1\,.\end{aligned}$$

This problem is a convex program since the objective is convex and the constraints are linear.[6] Hence, $\mathscr{P}_{\mathrm{sc}}$ can be solved using conventional convex optimization methods. In particular, such a problem can be transformed into a semidefinite program (SDP) or a second order cone program (SOCP) [41], which are more favorable formulations due to their efficient solvers [80]. The transformation of $\mathscr{P}_{\mathrm{sc}}$ into an SOCP will be described later on in this section.

Let $\boldsymbol{u}^* = [\,u_0^*, u_1^*, \ldots, u_{M-1}^*]^{\mathrm{T}}$ denote the optimal solution of $\mathscr{P}_{\mathrm{sc}}$. This solution can contain fractional elements due to the relaxation of the Boolean constraints and may not be feasible for $\mathscr{P}_{\mathrm{s}}$. Nonetheless, the optimal solution $\boldsymbol{u}^*$ can be employed to obtain a near-optimal selection of the assisting node positions. Consider the feasible solution $\mathring{\boldsymbol{u}} = [\,\mathring{u}_0, \mathring{u}_1, \ldots, \mathring{u}_{M-1}]^{\mathrm{T}}$ whose elements are given by

$$\mathring{u}_m = \begin{cases} 1 & \text{if } u_m^* \text{ is one of the } N_{\mathrm{c}} \text{ largest elements of } \boldsymbol{u}^* \\ 0 & \text{otherwise} \end{cases} \tag{21}$$

in which ties are broken arbitrarily.[7] In addition to determining a near-optimal solution to the node deployment problem by means of the rounding function in (21), solving the convex relaxation also provides a theoretical limit on the localization accuracy provided by assisting nodes given a finite set of candidate positions. In particular, the optimal objective of $\mathscr{P}_{\mathrm{sc}}$ cannot be greater than that of $\mathscr{P}_{\mathrm{s}}$ since the set of feasible solutions of $\mathscr{P}_{\mathrm{s}}$ is a subset of that of $\mathscr{P}_{\mathrm{sc}}$. Hence, we have the theoretical limit

$$\check{\mathcal{P}}(\mathring{\boldsymbol{u}};\boldsymbol{p}_0) \geqslant \check{\mathcal{P}}(\boldsymbol{u}^*;\boldsymbol{p}_0)\,. \tag{22}$$

This lower bound is useful to evaluate the near-optimal selection of assisting node positions determined by $\mathring{\boldsymbol{u}}$. For a certain instance of $\mathscr{P}_{\mathrm{s}}$, the gap between the position errors described by $\mathring{\boldsymbol{u}}$ and $\boldsymbol{u}^*$ is given by

$$\Delta_{\mathrm{c}} = \sqrt{\check{\mathcal{P}}(\mathring{\boldsymbol{u}};\boldsymbol{p}_0)} - \sqrt{\check{\mathcal{P}}(\boldsymbol{u}^*;\boldsymbol{p}_0)}\,. \tag{23}$$

Note that $\mathring{\boldsymbol{u}}$ is the optimal solution of $\mathscr{P}_{\mathrm{s}}$ if $\Delta_{\mathrm{c}} = 0$.

6. In convex optimization problems, any locally optimal solution is also globally optimal [80].

7. More sophisticated methods can be used to generate a feasible solution for $\mathscr{P}_{\mathrm{s}}$ based on the solution of its convex relaxation [77].

Next, we describe the transformation of $\mathscr{P}_{\mathrm{sc}}$ into an SOCP. First, the SPEB is rewritten in a matrix form as shown in the following proposition.

Proposition 1. The SPEB $\check{\mathcal{P}}(\boldsymbol{u};\boldsymbol{p}_0)$ can be written as

$$\check{\mathcal{P}}(\boldsymbol{u};\boldsymbol{p}_0) = \frac{4\,(\mathbf{1}^{\mathrm{T}}\boldsymbol{R}\boldsymbol{v})}{\boldsymbol{v}^{\mathrm{T}}\boldsymbol{R}^{\mathrm{T}}(\mathbf{1}\mathbf{1}^{\mathrm{T}} - \boldsymbol{c}\boldsymbol{c}^{\mathrm{T}} - \boldsymbol{s}\boldsymbol{s}^{\mathrm{T}})\boldsymbol{R}\boldsymbol{v}} \tag{24}$$

where

$$\begin{aligned}\boldsymbol{R} &= \operatorname{diag}\{\,\check{\xi}_0, \check{\xi}_1, \ldots, \check{\xi}_{M-1}, \lambda_{0,1}, \lambda_{0,2}, \ldots, \lambda_{0,N_{\mathrm{b}}}\} \\ \boldsymbol{v} &= [\,\boldsymbol{u}^{\mathrm{T}}, \mathbf{1}_{N_{\mathrm{b}}}^{\mathrm{T}}]^{\mathrm{T}} \\ \boldsymbol{c} &= [\,\boldsymbol{c}_{\mathrm{c}}^{\mathrm{T}}, \boldsymbol{c}_{\mathrm{b}}^{\mathrm{T}}]^{\mathrm{T}} \\ \boldsymbol{s} &= [\,\boldsymbol{s}_{\mathrm{c}}^{\mathrm{T}}, \boldsymbol{s}_{\mathrm{b}}^{\mathrm{T}}]^{\mathrm{T}} \\ \boldsymbol{c}_{\mathrm{c}} &= [\,\cos(2\theta_0), \cos(2\theta_1), \ldots, \cos(2\theta_{M-1})]^{\mathrm{T}} \\ \boldsymbol{c}_{\mathrm{b}} &= [\,\cos(2\phi_{0,1}), \cos(2\phi_{0,2}), \ldots, \cos(2\phi_{0,N_{\mathrm{b}}})]^{\mathrm{T}} \\ \boldsymbol{s}_{\mathrm{c}} &= [\,\sin(2\theta_0), \sin(2\theta_1), \ldots, \sin(2\theta_{M-1})]^{\mathrm{T}} \\ \boldsymbol{s}_{\mathrm{b}} &= [\,\sin(2\phi_{0,1}), \sin(2\phi_{0,2}), \ldots, \sin(2\phi_{0,N_{\mathrm{b}}})]^{\mathrm{T}}\,.\end{aligned}$$

Proof: The 2×2 EFIM $\check{\boldsymbol{J}}_{\mathrm{e}}(\boldsymbol{u};\boldsymbol{p}_0)$ can be written as

$$\check{\boldsymbol{J}}_{\mathrm{e}}(\boldsymbol{u};\boldsymbol{p}_0) = \begin{bmatrix} a_{\mathrm{e}} & b_{\mathrm{e}} \\ b_{\mathrm{e}} & d_{\mathrm{e}} \end{bmatrix}$$

where

$$\begin{aligned}a_{\mathrm{e}} &= \sum_{m=0}^{M-1} u_m \check{\xi}_m \cos^2(\theta_m) + \sum_{i=1}^{N_{\mathrm{b}}} \lambda_{0,i} \cos^2(\phi_{0,i}) \\ b_{\mathrm{e}} &= \sum_{m=0}^{M-1} u_m \check{\xi}_m \cos(\theta_m)\sin(\theta_m) + \sum_{i=1}^{N_{\mathrm{b}}} \lambda_{0,i} \cos(\phi_{0,i})\sin(\phi_{0,i}) \\ d_{\mathrm{e}} &= \sum_{m=0}^{M-1} u_m \check{\xi}_m \sin^2(\theta_m) + \sum_{i=1}^{N_{\mathrm{b}}} \lambda_{0,i} \sin^2(\phi_{0,i})\,.\end{aligned}$$

Considering the formula for the inverse of a 2×2 matrix, the SPEB is given by

$$\check{\mathcal{P}}(\boldsymbol{u};\boldsymbol{p}_0) = \frac{a_{\mathrm{e}} + d_{\mathrm{e}}}{a_{\mathrm{e}}d_{\mathrm{e}} - b_{\mathrm{e}}^2}\,. \tag{25}$$

We obtain (24) after some algebra considering trigonometric identities and rewriting in terms of $\boldsymbol{R}$, $\boldsymbol{v}$, $\boldsymbol{c}$, and $\boldsymbol{s}$. □

The following proposition provides the transformation of $\mathscr{P}_{\mathrm{sc}}$ into an SOCP.

Proposition 2 (SOCP). The problem $\mathscr{P}_{\mathrm{sc}}$ is equivalent to the SOCP

$$\begin{aligned}\mathscr{P}_{\mathrm{sc}}^{\mathrm{SOCP}}\colon \ \underset{\boldsymbol{u},\,\varrho,\,\sigma}{\text{minimize}} \quad & \varrho \\ \text{subject to} \quad & \|\boldsymbol{A}\boldsymbol{R}\boldsymbol{v} + \boldsymbol{b}\| \leqslant \mathbf{1}^{\mathrm{T}}\boldsymbol{R}\boldsymbol{v} - 2\sigma \\ & \left\|\left[\,\sigma, \varrho, \sqrt{2}\,\right]^{\mathrm{T}}\right\| \leqslant \sigma + \varrho \\ & \mathbf{1}^{\mathrm{T}}\boldsymbol{u} = N_{\mathrm{c}} \\ & -\boldsymbol{u} \preccurlyeq \boldsymbol{0} \\ & \boldsymbol{u} \preccurlyeq \boldsymbol{1}\end{aligned}$$

where $\boldsymbol{A} = [\boldsymbol{c}, \boldsymbol{s}, \boldsymbol{0}]^{\mathrm{T}}$ and $\boldsymbol{b} = [0, 0, 2\sigma]^{\mathrm{T}}$.

Proof: The problem $\mathscr{P}_{\mathrm{sc}}$ can be rewritten as

$$\begin{aligned}\underset{\boldsymbol{u},\,\varrho}{\text{minimize}} \quad & \varrho \\ \text{subject to} \quad & \check{\mathcal{P}}(\boldsymbol{u};\boldsymbol{p}_0) \leqslant \varrho \\ & \mathbf{1}^{\mathrm{T}}\boldsymbol{u} = N_{\mathrm{c}} \\ & -\boldsymbol{u} \preccurlyeq \boldsymbol{0} \\ & \boldsymbol{u} \preccurlyeq \boldsymbol{1}\,.\end{aligned}$$

Algorithm 2 SOCP-based Node Deployment Strategy

Input: Target agent position $\boldsymbol{p}_0$, deployment regions $\mathcal{R}_1, \mathcal{R}_2, \ldots, \mathcal{R}_K$, number of candidate positions M, and number of assisting nodes N_c.

Output: Assisting node positions $\boldsymbol{p}_\mathrm{c}$.

1: Determine candidate positions $\check{\boldsymbol{p}}_\mathrm{c}$ and ERCs $\check{\boldsymbol{\xi}}_\mathrm{c}$ based on Algorithm 1.
2: Solve $\mathscr{P}_\mathrm{sc}^{\mathrm{SOCP}}$ to determine the solution $\boldsymbol{u}^*$.
3: Generate the near-optimal feasible solution $\mathring{\boldsymbol{u}}$ based on $\boldsymbol{u}^*$ by evaluating (21).
4: Determine $\boldsymbol{p}_\mathrm{c}$ based on $\check{\boldsymbol{p}}_\mathrm{c}$ and $\mathring{\boldsymbol{u}}$.

From (24), the constraint on $\check{\mathcal{P}}(\boldsymbol{u}; \boldsymbol{p}_0)$ can be rewritten as

$$\frac{4}{\varrho}(\mathbf{1}^\mathrm{T}\boldsymbol{R}\boldsymbol{v}) \leqslant (\mathbf{1}^\mathrm{T}\boldsymbol{R}\boldsymbol{v})^2 - (\boldsymbol{c}^\mathrm{T}\boldsymbol{R}\boldsymbol{v})^2 - (\boldsymbol{s}^\mathrm{T}\boldsymbol{R}\boldsymbol{v})^2 .$$

Then, we have

$$(\boldsymbol{c}^\mathrm{T}\boldsymbol{R}\boldsymbol{v})^2 + (\boldsymbol{s}^\mathrm{T}\boldsymbol{R}\boldsymbol{v})^2 \leqslant (\mathbf{1}^\mathrm{T}\boldsymbol{R}\boldsymbol{v})^2 - \frac{4}{\varrho}(\mathbf{1}^\mathrm{T}\boldsymbol{R}\boldsymbol{v})$$

and, by completing the square in the right side

$$(\boldsymbol{c}^\mathrm{T}\boldsymbol{R}\boldsymbol{v})^2 + (\boldsymbol{s}^\mathrm{T}\boldsymbol{R}\boldsymbol{v})^2 + \frac{4}{\varrho^2} \leqslant (\mathbf{1}^\mathrm{T}\boldsymbol{R}\boldsymbol{v})^2 - \frac{4}{\varrho}(\mathbf{1}^\mathrm{T}\boldsymbol{R}\boldsymbol{v}) + \frac{4}{\varrho^2} .$$

Since $\mathbf{1}^\mathrm{T}\boldsymbol{R}\boldsymbol{v} - 2/\varrho \geqslant 0$, this inequality can be rewritten as

$$\left\| [\, \boldsymbol{c}^\mathrm{T}\boldsymbol{R}\boldsymbol{v}, \boldsymbol{s}^\mathrm{T}\boldsymbol{R}\boldsymbol{v}, 2\sigma \,]^\mathrm{T} \right\| \leqslant \mathbf{1}^\mathrm{T}\boldsymbol{R}\boldsymbol{v} - 2\sigma \tag{26}$$

where $\sigma = 1/\varrho$. The constraint $\sigma = 1/\varrho$ can be transformed, without changing the optimal solution, into

$$\left\| [\, \sigma, \varrho, \sqrt{2} \,]^\mathrm{T} \right\| \leqslant \sigma + \varrho .$$

The proof is completed by rewriting the inequality (26) in terms of $\boldsymbol{A}$ and $\boldsymbol{b}$. □

Algorithm 2 presents the SOCP-based node deployment strategy. Specifically, solving the SOCP requires the implementation of an iterative optimization algorithm (e.g., an interior-point method) or the use of a convex optimization engine (e.g., CVX [86]).

Remark 1 (Complexity). Standard form SOCPs can be solved efficiently via interior-point methods [80]. In particular, solving $\mathscr{P}_\mathrm{sc}^{\mathrm{SOCP}}$ with an interior-point method has a worst-case complexity of $O((M + N_\mathrm{b})^3)$ since the dimension of $\boldsymbol{v}$ is $M + N_\mathrm{b}$ [87].

5 ADP Algorithm

The SOCP-based node deployment strategy described in Section 4 requires a convex optimization engine and a rounding function to determine near-optimal assisting node positions. While such a strategy can provide reliable solutions for the near-optimal deployment of assisting nodes, other approaches can be employed to design approximate algorithms with more amenable complexity and without relying on sophisticated optimization solvers. Next, we develop an ADP algorithm for deploying assisting nodes.[8]

8. While the focus remains on the node deployment problem of assisting nodes, the ADP algorithm developed in this section can be applied to other selection problems.

Consider the formulation of the node deployment problem after discretizing the set of possible positions and with the determinant of the EFIM for the position of the target agent as localization performance metric. This optimization problem is expressed as

$$\begin{aligned} \underset{\boldsymbol{u}}{\text{minimize}} \quad & -\check{\mathcal{Q}}(\boldsymbol{u}; \boldsymbol{p}_0) \\ \text{subject to} \quad & \mathbf{1}^\mathrm{T}\boldsymbol{u} = N_\mathrm{c} \\ & u_m \in \{0, 1\}, \;\; m = 0, 1, \ldots, M-1 . \end{aligned}$$

With this problem formulation, the node deployment strategy aims to select the N_c positions where assisting nodes should be deployed to maximize the confidence of the position estimator $\hat{\mathbf{p}}_0$. We propose solving this problem approximately via dynamic programming.

In dynamic programming algorithms, decisions are made in stages [88], [89], [90]. In our formulation, stages are related to the indices of the candidate positions. Consider a finite horizon problem with $M+1$ stages in which the last stage incorporates the position information obtained from anchors. Let x_m for $m = 0, 1, \ldots, M$ and $u_m \in \mathcal{U}_m(x_m)$ for $m = 0, 1, \ldots, M-1$ denote the state and decision variables, where $\mathcal{U}_m(x_m)$ is the constraint set at stage m. Specifically, x_m is a non-negative integer that encodes the number of available assisting nodes at stage m; and u_m encodes whether an assisting node is deployed at the candidate position $\check{\boldsymbol{p}}_m$ or not. The initial condition is $x_0 = N_\mathrm{c}$ assisting nodes. In addition, the constraint set at stage m is given by

$$\mathcal{U}_m(x_m) = \begin{cases} \{0, 1\} & \text{if} \quad x_m > 0 \\ \{0\} & \text{otherwise} \end{cases} \tag{27}$$

and the state transitions are given by $x_{m+1} = x_m - u_m$.

A key aspect of dynamic programming is that it requires an additive objective function of the form [88], [89], [90]

$$G(x_0; u_0, u_1, \ldots, u_{M-1}) = g_M(x_M) + \sum_{m=0}^{M-1} g_m(x_m, u_m) \tag{28}$$

where $g_M(x_M)$ is the terminal objective incurred at the last stage, and $g_m(x_m, u_m)$ is the objective at stage m. Fig. 4 illustrates the transition graph of the node deployment problem for two assisting nodes, (i.e., $x_0 = 2$). In this diagram, nodes and arcs represent states and possible state transitions, respectively. The state transitions have an associated objective $g_m(x_m, u_m)$ (or $g_M(x_M)$ for the final stage). Note that an artificial node representing the terminal state, T, is added to incorporate the terminal objective. Furthermore, possible solutions correspond to trajectories from the initial stage to the last stage. For example, the possible decisions at the first stage are: (a) to not deploy an assisting node at $\check{\boldsymbol{p}}_0$ with objective $g_0(2, 0)$, or (b) to deploy an assisting node at $\check{\boldsymbol{p}}_0$ with objective $g_0(2, 1)$; which will result in having either two or one assisting nodes available at the next stage, respectively. After choosing a decision, the sequence proceeds similarly until the last stage adding the terminal objective.

The matrix determinant lemma [91] provides a useful expression to develop the ADP algorithm. For an invertible $n \times n$ matrix $\boldsymbol{\Lambda}$ and n-dimensional vectors $\boldsymbol{x}$ and $\boldsymbol{y}$, the

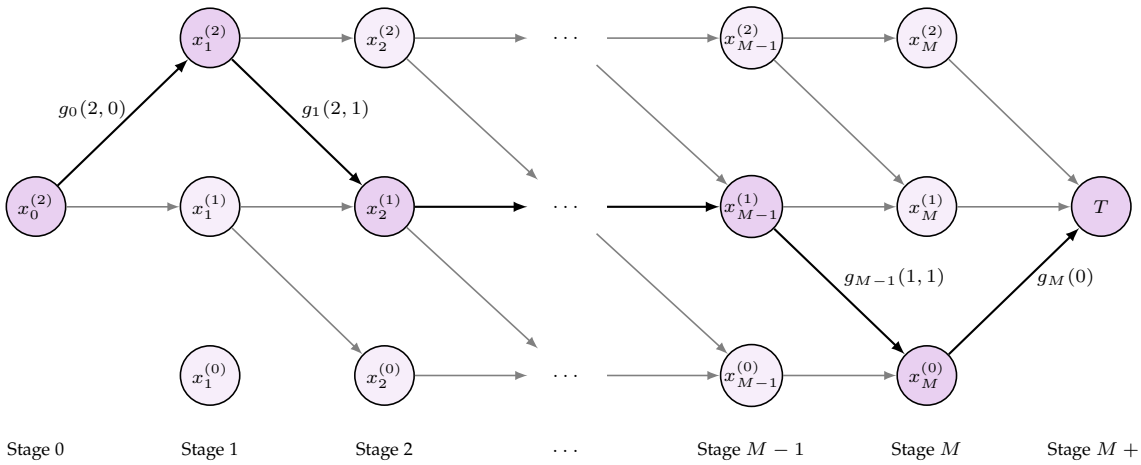

Fig. 4. Transition graph for the node deployment problem with $x_0 = 2$ assisting nodes and M candidate positions. Notation $x_i^{(k)}$ denotes the state $x_i = k$. Black solid lines represent a solution to the problem, and the functions on its arcs are the objectives of the corresponding state transitions.

logarithmic form of the matrix determinant lemma provides an additive expression given by

$$\log\big[\det\{\boldsymbol{\Lambda} + \boldsymbol{x}\boldsymbol{y}^{\mathrm{T}}\}\big] = \log\big[1 + \boldsymbol{y}^{\mathrm{T}}\boldsymbol{\Lambda}^{-1}\boldsymbol{x}\big] + \log\big[\det\{\boldsymbol{\Lambda}\}\big]\,. \tag{29}$$

Expressions of this form can be used recursively to compute the log-determinant of $\check{\boldsymbol{J}}_{\mathrm{e}}(\boldsymbol{u};\boldsymbol{p}_0)$, i.e., $\log[\check{\mathcal{Q}}(\boldsymbol{u};\boldsymbol{p}_0)]$. Note that $\boldsymbol{J}_{\mathrm{r}}(\phi)$ can be rewritten as [76]

$$\boldsymbol{J}_{\mathrm{r}}(\phi) = \boldsymbol{q}(\phi)\boldsymbol{q}(\phi)^{\mathrm{T}} \tag{30}$$

where $\boldsymbol{q}(\phi) = [\cos(\phi), \sin(\phi)]^{\mathrm{T}}$. An assisting node placed at the candidate position $\check{\boldsymbol{p}}_m$ will provide the target agent with position information equal to $\check{\xi}_m\boldsymbol{q}(\theta_m)\boldsymbol{q}(\theta_m)^{\mathrm{T}}$.

Since the goal is to maximize the area of the information ellipse, consider the minimization of $-\log\big[\check{\mathcal{Q}}(\boldsymbol{u};\boldsymbol{p}_0)\big]$ over $M+1$ stages as described by (28). Considering that $\boldsymbol{J}_{\mathrm{e}}^{\mathrm{A}}(\boldsymbol{p}_0)$ is non-singular, the terminal objective is given by

$$g_M(x_M) = -\log\Big[\det\big\{\boldsymbol{J}_{\mathrm{e}}^{\mathrm{A}}(\boldsymbol{p}_0)\big\}\Big]\,. \tag{31}$$

Then, the objective of stage m can be formulated considering the EFIM that accumulates from stage $m+1$ to stage M as

$$g_m(x_m, u_m) = \\ -\log\big[1 + u_m\check{\xi}_m\boldsymbol{q}(\theta_m)^{\mathrm{T}}\{\check{\boldsymbol{J}}_{m+1}(x_m - u_m)\}^{-1}\boldsymbol{q}(\theta_m)\big] \tag{32}$$

for $m = 0, 1, \ldots, M-1$, where $\check{\boldsymbol{J}}_{m+1}(x_m - u_m)$ is the EFIM that accumulates from stage $m+1$ to stage M when $x_m - u_m$ assisting nodes are available at stage $m+1$. In particular,

$$\check{\boldsymbol{J}}_{m+1}(x_m - u_m) = \boldsymbol{J}_{\mathrm{e}}^{\mathrm{A}}(\boldsymbol{p}_0) + \sum_{i=m+1}^{M-1} u_i\check{\xi}_i\boldsymbol{J}_{\mathrm{r}}(\theta_i) \tag{33}$$

where u_i is the decision made at stage i.

The starting point of the ADP algorithm is given by

$$D_M(x_M) = g_M(x_M) \tag{34}$$

for $x_M = 0, 1, \ldots, N_{\mathrm{c}}$. Moreover, the tail subproblems for the rest of the stages take the form

$$D_m(x_m) = \min_{u_m \in \mathcal{U}_m(x_m)} \big\{g_m(x_m, u_m) + D_{m+1}(x_m - u_m)\big\}\,. \tag{35}$$

For the intermediate stages, $m = 1, 2, \ldots, M-1$, the state x_m can take the values in the set $\{0, 1, \ldots, N_{\mathrm{c}}\}$. Since the optimal objective of the problem is equal to $D_0(x_0)$, the tail subproblem at the first stage is solved only for $x_0 = N_{\mathrm{c}}$ assisting nodes. The solution of the ADP algorithm, denoted by $\check{\boldsymbol{u}} = [\,\check{u}_0, \check{u}_1, \ldots, \check{u}_{M-1}]^{\mathrm{T}}$, is determined starting from the first stage and proceeding forward [88], [89], [90].

We can compare the position error determined by the solution of the ADP-based node deployment strategy with the theoretical limit provided by solving the convex relaxation presented in Section 4. The gap between the position errors determined by $\check{\boldsymbol{u}}$ and $\boldsymbol{u}^*$ is given by

$$\Delta_{\mathrm{ADP}} = \sqrt{\check{\mathcal{P}}(\check{\boldsymbol{u}};\boldsymbol{p}_0)} - \sqrt{\check{\mathcal{P}}(\boldsymbol{u}^*;\boldsymbol{p}_0)}\,. \tag{36}$$

Note that $\check{\boldsymbol{u}}$ is the optimal solution to the node deployment problem of assisting nodes in terms of the position error if $\Delta_{\mathrm{ADP}} = 0$.

Algorithm 3 presents the ADP-based node deployment strategy. Specifically, solving the proposed ADP recursion requires the evaluation of arithmetic operations and the storage of intermediate results. Note that the ADP algorithm does not require evaluating all the possible solutions of the combinatorial problem as in an exhaustive search approach.

Remark 2 (Complexity). The complexity of the ADP algorithm can be analyzed by considering the number of tail subproblems that need to be solved. In the last stage, $D_M(x_M)$ is computed only once with a constant running time since $g_M(x_M)$ is invariant with x_M. For the intermediate stages, $M-1$ tail subproblems of the form of (35) need to be solved for $N_{\mathrm{c}}+1$ possible states, i.e., for a total of $(M-1)(N_{\mathrm{c}}+1)$ tail subproblems. Finally, a single tail subproblem is solved at the first stage. Considering that all the tail subproblems are solved with worst-case complexity, the ADP algorithm has worst-case complexity of $O(MN_{\mathrm{c}})$. Thus, for a given N_{c}, the complexity of the ADP algorithm is linear on M. Note that the worst-case complexity of the ADP algorithm is upper bounded by $O(M^2)$ since $N_{\mathrm{c}} \leqslant M$ from the problem formulation. Therefore, the ADP-based node deployment strategy has a more amenable complexity compared to the SOCP-based strategy with worst-case complexity of $O((M+N_{\mathrm{b}})^3)$.

Algorithm 3 ADP-based Node Deployment Strategy

Input: Target agent position $\boldsymbol{p}_0$, deployment regions $\mathcal{R}_1, \mathcal{R}_2, \ldots, \mathcal{R}_K$, number of candidate positions M, and number of assisting nodes N_c.

Output: Assisting node positions $\boldsymbol{p}_\mathrm{c}$.

1: Determine candidate positions $\check{\boldsymbol{p}}_\mathrm{c}$ and ERCs $\check{\boldsymbol{\xi}}_\mathrm{c}$ based on Algorithm 1.
2: Compute $D_M(x_M)$ for the last stage given by (34).
3: Perform the ADP recursion (35) backward for the intermediate stages starting from $D_M(x_M)$.
4: Solve $D_0(N_\mathrm{c})$ and determine $\check{\boldsymbol{u}}$ proceeding forward.
5: Determine $\boldsymbol{p}_\mathrm{c}$ based on $\check{\boldsymbol{p}}_\mathrm{c}$ and $\check{\boldsymbol{u}}$.

6 Inverse Node Deployment Problem

The methodology developed in this paper is also applicable to other formulations of the node deployment problem. Consider the inverse node deployment problem in which the goal is to determine the minimum number of assisting nodes that are needed to meet a localization performance requirement. The solution to this problem not only establishes how many assisting nodes are needed, but also dictates where to deploy them. Let $\overleftarrow{\mathscr{P}}$ denote the inverse node deployment problem of assisting nodes expressed as

$$\overleftarrow{\mathscr{P}}\colon \underset{N_\mathrm{c},\,\boldsymbol{p}_\mathrm{c}}{\text{minimize}} \quad N_\mathrm{c} \tag{37a}$$

$$\text{subject to} \quad \mathcal{P}(\boldsymbol{p}_\mathrm{c};\boldsymbol{p}_0) \leqslant \varrho_\mathrm{r} \tag{37b}$$

$$\boldsymbol{p}_i \in \mathcal{S}, \quad i \in \mathcal{N}_\mathrm{c} \tag{37c}$$

where the constraint (37b) establishes the localization performance requirement in terms of the SPEB. In this constraint, ϱ_r is a predefined performance threshold describing the required SPEB. Furthermore, the localization performance requirement can also be expressed in terms of $\mathcal{Q}(\boldsymbol{p}_\mathrm{c};\boldsymbol{p}_0)$. In the latter case, the constraint (37b) is replaced by $\mathcal{Q}(\boldsymbol{p}_\mathrm{c};\boldsymbol{p}_0) \geqslant \zeta_\mathrm{r}$, where ζ_r is a predefined performance threshold describing the required determinant of the EFIM for the position of the target agent. Next, we describe two approaches for solving the inverse node deployment problem based on convex optimization and ADP, respectively.

6.1 Convex Relaxation

Consider the formulation of the inverse node deployment problem after the discretization of the set of possible assisting node positions. This problem is expressed as

$$\overleftarrow{\mathscr{P}}_\mathrm{s}\colon \underset{\boldsymbol{u}}{\text{minimize}} \quad \mathbf{1}^\mathrm{T}\boldsymbol{u} \tag{38a}$$

$$\text{subject to} \quad \check{\mathcal{P}}(\boldsymbol{u};\boldsymbol{p}_0) \leqslant \varrho_\mathrm{r} \tag{38b}$$

$$u_m \in \{0,1\}, \quad m = 0,1,\ldots,M-1 \tag{38c}$$

where $\overleftarrow{\mathscr{P}}_\mathrm{s}$ denotes the formulation of the problem $\overleftarrow{\mathscr{P}}$ as a selection problem. This problem may be viewed as a relaxation of $\overleftarrow{\mathscr{P}}$ since it considers a finite subset of possible assisting node positions. Note that the objective of $\overleftarrow{\mathscr{P}}_\mathrm{s}$ is upper bounded by M, which is the dimension of $\boldsymbol{u}$.

Since $\check{\mathcal{P}}(\boldsymbol{u};\boldsymbol{p}_0)$ is convex for $\boldsymbol{u} \succcurlyeq \mathbf{0}$, the convex relaxation of the inverse node deployment problem can be obtained by replacing the Boolean constraints in (38c) with the box constraints $0 \leqslant u_m \leqslant 1$. Let $\overleftarrow{\boldsymbol{u}}^*$ denote the optimal solution to the convex relaxation of $\overleftarrow{\mathscr{P}}_\mathrm{s}$. This solution may not be feasible to the integer problem since it can contain fractional elements. We consider the near-optimal feasible solution whose elements correspond to the entries of $\overleftarrow{\boldsymbol{u}}^*$ after applying an element-wise ceiling function. The optimal objective of $\overleftarrow{\mathscr{P}}_\mathrm{s}$ is lower bounded by $\mathbf{1}^\mathrm{T}\overleftarrow{\boldsymbol{u}}^*$ since the set of feasible solutions of the integer problem is a subset of that of its convex relaxation.

The convex relaxation of the problem $\overleftarrow{\mathscr{P}}_\mathrm{s}$ can be transformed into an SOCP as shown in the next proposition.

Proposition 3 (SOCP for the inverse problem). The convex relaxation of $\overleftarrow{\mathscr{P}}_\mathrm{s}$ is equivalent to the SOCP

$$\overleftarrow{\mathscr{P}}_\mathrm{s\,c}^{\mathrm{SOCP}}\colon \underset{\boldsymbol{u}}{\text{minimize}} \quad \mathbf{1}^\mathrm{T}\boldsymbol{u}$$

$$\text{subject to} \quad \|\boldsymbol{A}\boldsymbol{R}\boldsymbol{v} + \boldsymbol{b}\| \leqslant \mathbf{1}^\mathrm{T}\boldsymbol{R}\boldsymbol{v} - 2/\varrho_\mathrm{r}$$

$$-\boldsymbol{u} \preccurlyeq \mathbf{0}$$

$$\boldsymbol{u} \preccurlyeq \mathbf{1}$$

where $\boldsymbol{A} = [\boldsymbol{c}, \boldsymbol{s}, \mathbf{0}]^\mathrm{T}$ and $\boldsymbol{b} = [0, 0, 2/\varrho_\mathrm{r}]^\mathrm{T}$.

Proof: The proof follows the same approach of that for Proposition 2. □

6.2 ADP Algorithm

The inverse node deployment problem can also be formulated with $\mathcal{Q}(\boldsymbol{p}_\mathrm{c};\boldsymbol{p}_0)$ as localization performance metric. After discretizing the set of possible assisting node positions, the inverse node deployment problem can be formulated similarly to $\overleftarrow{\mathscr{P}}_\mathrm{s}$ by replacing (38b) with $\mathcal{Q}(\boldsymbol{p}_\mathrm{c};\boldsymbol{p}_0) \geqslant \zeta_\mathrm{r}$. This optimization problem can be solved using the ADP recursion described by (34) and (35) considering a range of initial conditions. Let $\check{N}$ be an upper bound for the state x_0. The starting point of the ADP algorithm for the inverse deployment problem is given by (34) for $x_M = 0, 1, \ldots, \check{N}$, and the tail subproblems take the form of (35) for the rest of the stages. In the inverse node deployment problem, the state x_m can take the values in the set $\{0, 1, \ldots, \check{N}\}$ for $m = 0, 1, \ldots, M-1$. After computing the tail subproblems at the first stage, the next step consists of searching for the smallest value of x_0 that satisfies $D_0(x_0) \leqslant -\log(\zeta_\mathrm{r})$, i.e., the minimum number of assisting nodes that meet the required performance. Finally, the solution is determined starting from that initial condition and proceeding forward.

7 Case Study

This section evaluates the performance of the developed node deployment strategies in a case study.

Consider a location-aware network composed of ultra-wideband (UWB) nodes. The UWB technology [92], [93], [94], [95], [96] is readily available in consumer devices, and the deployment of UWB assisting nodes can enable high-accuracy localization in 5G and beyond ecosystems [12], [13], [97]. Specifically, we consider a 3GPP indoor open office scenario in which anchors are placed according to the layout in [98], and assisting nodes are additionally deployed therein to improve the localization accuracy of a target agent. Consider the cases: (C1) full anchor deployment, in which all anchors in the standard indoor open office layout

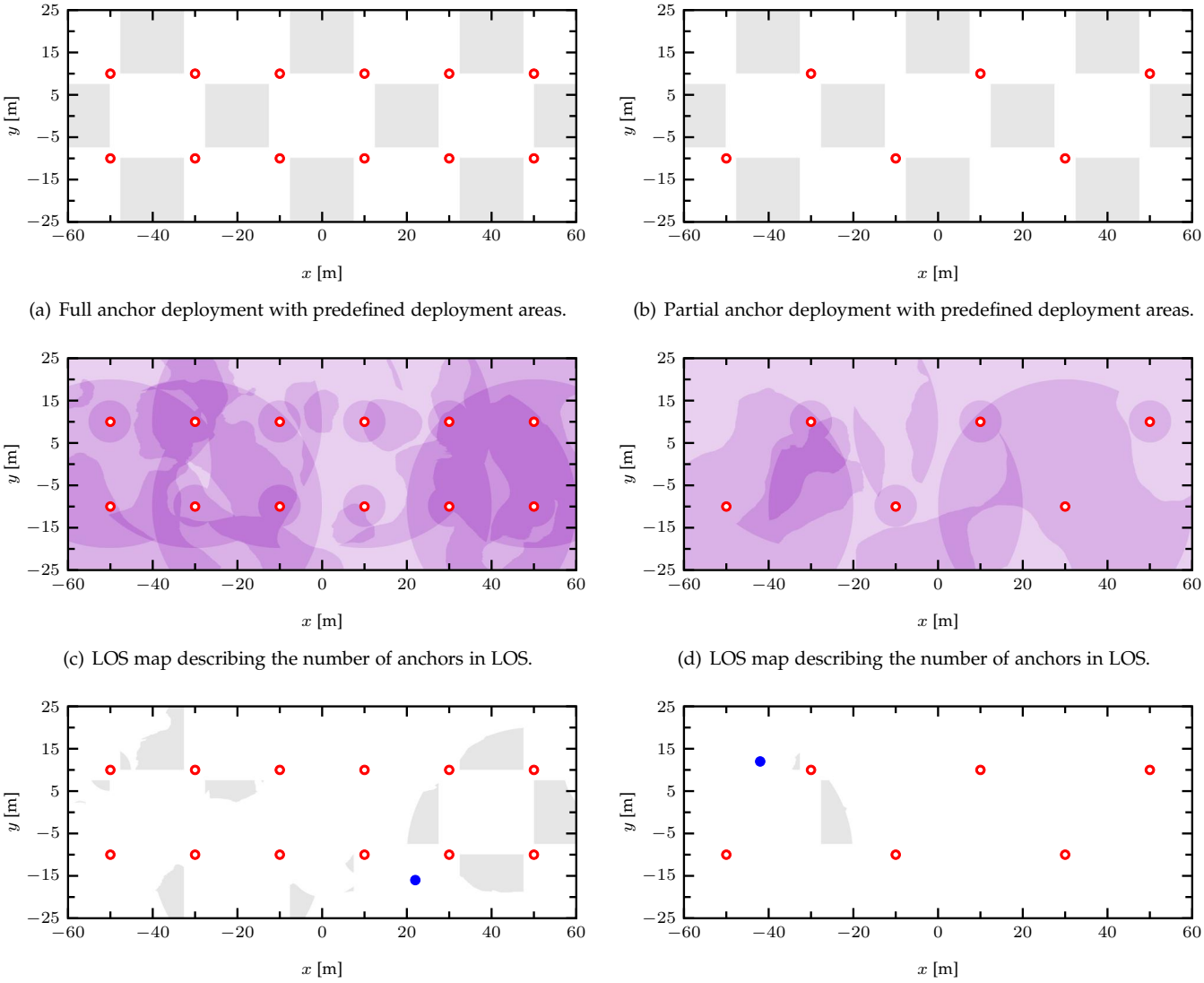

(a) Full anchor deployment with predefined deployment areas.

(b) Partial anchor deployment with predefined deployment areas.

(c) LOS map describing the number of anchors in LOS.

(d) LOS map describing the number of anchors in LOS.

(e) Simulation scenario after determining the deployment regions.

(f) Simulation scenario after determining the deployment regions.

Fig. 5. Simulation scenarios for cases C1 (left column) and C2 (right column). The predefined deployment areas (top) and realizations of the LOS map describing the number of anchors in LOS conditions observed from each position (center) determine the deployment regions (bottom). The four shades of lilac in the LOS maps depict the positions with zero (lightest), one, two, and at least three (darkest) anchors observed in LOS conditions.

are placed; and (C2) partial anchor deployment, in which half of those anchors are considered (see Fig. 5). Unless otherwise indicated, the results correspond to case C1. The nodes emit UWB root raised cosine pulses compliant with the IEEE 802.15.4a standard [99]. The multipath channels are modeled according to the IEEE 802.15.4a channel model for the indoor office scenario [100]. The noise figure, center frequency, and maximum power spectral density are 10 dB, 6.489 GHz, and -41.3 dBm/MHz, respectively [99]. The transmitting power of the target agent and assisting nodes is set to fractions of that of anchors, which is denoted as P_{b}.

Furthermore, we consider spatially-consistent wireless channels [101], [102].[9] Specifically, we consider spatially-consistent LOS/NLOS states and POCs.[10] The RII between nodes in NLOS conditions is set to zero. The deployment regions are determined as follows. First, maps of LOS/NLOS states from anchors and target agent are generated for the indoor open office scenario according to [101]. Then, the deployment regions are determined by the intersection between predefined deployment areas and the locations where assisting nodes will be in LOS conditions with the target agent and at least two anchors. In addition, POCs are generated for the IEEE 802.15.4a indoor office scenario following [85] and [102].

Fig. 5 shows realizations of the simulation scenario for the two considered cases. Anchors are deployed according to the indoor open office scenario, and ten predefined deployment areas are considered as map constraints for the positions of assisting nodes (see Figs. 5(a) and 5(b)). To determine the deployment regions, we consider realizations of LOS maps describing the number of anchors in LOS condition observed from each position (see Figs. 5(c) and 5(d)). These LOS maps show the areas where deploying assisting nodes can benefit accurate localization. For example,

9. Spatial consistency is not considered in the IEEE 802.15.4a channel model. We consider the parameters in [98].

10. Spatially-consistent POCs can be obtained by following the same approach of small-scale parameters [102].

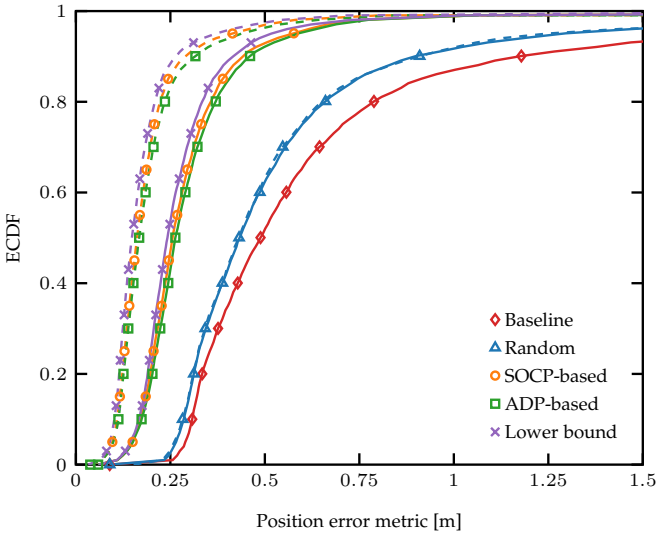

Fig. 6. ECDF of the position error metric for different node deployment strategies with $N_c = 2$ (solid line) and 8 (dashed line) assisting nodes. The performance is evaluated with $M = 16$ candidate positions. For the lower bound of the convex relaxation, $M = 128$ is considered.

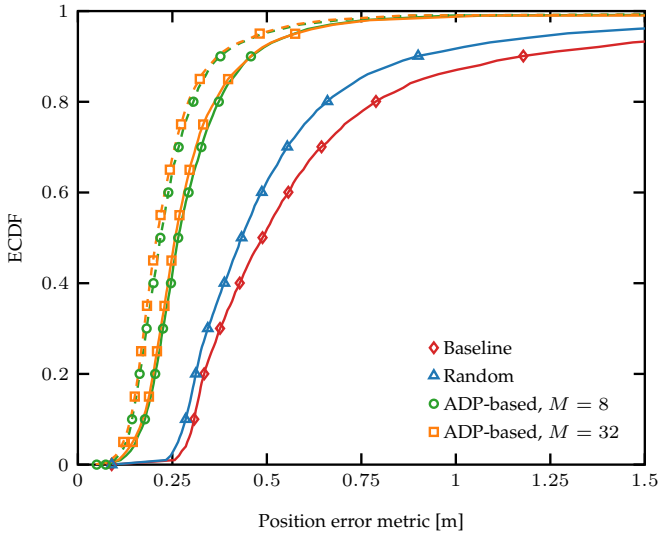

Fig. 7. ECDF of the position error metric for the ADP-based node deployment strategy with $M = 8$ and 32 candidate positions, and $N_c = 2$ (solid line) and 4 (dashed line) assisting nodes. For the random deployment strategy, $N_c = 2$ assisting nodes are considered.

agents may have inadequate localization performance in areas where less than three anchors are in LOS conditions. The deployment regions are determined by considering the intersection between the predefined deployment areas and the positions from which the target agent and at least two anchors will be observed in LOS conditions (see Figs. 5(e) and 5(f)). Note that these 3GPP scenarios highlight the importance of a general problem formulation with multiple deployment regions.

The case study focuses on revealing the benefits of assisting nodes for accurate localization in complex and infrastructure-limited wireless environments, especially if deployed according to near-optimal strategies. Furthermore, we evaluate the impact of different parameters on the localization performance provided by assisting nodes. The localization performance is evaluated using the empirical cumulative distribution function (ECDF) of the position error metric (the square root of the SPEB) over many instantiations of target agent positions and channel conditions. For the SOCP-based node deployment strategy, the optimization problems are solved using CVX [86]. We compare the performance of the developed strategies against both the baseline performance without deploying assisting nodes and the performance of the random deployment strategy in which assisting nodes are at uniformly random positions within the deployment regions. The baseline performance reveals the possible benefits of deploying assisting nodes since it is based only on the existing infrastructure. The random deployment strategy provides a benchmark to compare the performance with assisting nodes placed using near-optimal strategies. For these benchmarks, we consider that the target agent performs measurements with three active anchors and assisting nodes, if any. In contrast, the target agent performs measurements with at most two active anchors, which represents a worse case, and assisting nodes for the near-optimal node deployment strategies.

Fig. 6 shows the performance of the random, SOCP-based, and ADP-based strategies for deploying assisting nodes with the baseline performance and the theoretical limits provided by the solutions to the SOCP. The performance is evaluated for $N_c = 2$ and 8 assisting nodes with $M = 16$ candidate positions and $P_c = 0.5P_b$. Note that the proposed strategies provide a significant performance improvement over the baseline and the random deployment strategy. For example, the position errors for the baseline performance, and the random and ADP-based deployment strategies with $N_c = 2$ assisting nodes are below 1.17 m, below 0.90 m, and below 0.46 m, respectively, for 90% of the cases. At this mark, the random and ADP-based strategies reduce the position error by 23% and 61% over the baseline performance, respectively. In addition, note that the ADP-based strategy provides adequate performance since the gaps with respect to the SOCP-based strategy and the lower bound are small. In particular, the sample mean values of Δ_{ADP} with $M = 16$ are 0.02 m and 0.01 m for $N_c = 2$ and 8 assisting nodes, respectively. Note that, regardless the specific choice of technology, the performance improvements provided by the proposed strategies are due to the near-optimal selection of the assisting nodes positions. In the following, the results focus on the ADP-based strategy.

Fig. 7 shows the performance of the ADP-based strategy for deploying assisting nodes with $M = 8$ and 32 candidate positions. The performance is evaluated for $N_c = 2$ and 4 assisting nodes with $P_c = 0.5P_b$. The baseline performance and the random deployment strategy with $N_c = 2$ assisting nodes are shown as benchmarks. Note that increasing the number of assisting nodes reduces the position error. However, a significant performance improvement can also be obtained with a small number of assisting nodes (e.g., $N_c = 2$). Observe also that increasing M can improve the performance further due to a better approximation of the deployment problem. Nonetheless, adequate performance can be obtained with small values of M (e.g., $M = 8$). For example, the position errors using $N_c = 4$ assisting nodes with $M = 8$ and 32 are below 0.38 m and below 0.36 m, respectively, for 90% of the cases. This represents

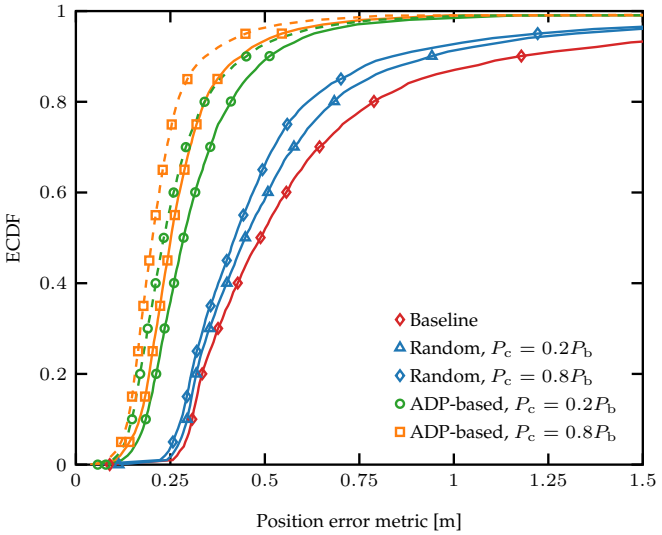

Fig. 8. ECDF of the position error metric for the ADP-based node deployment strategy with $P_c = 0.2P_b$ and $0.8P_b$, and $N_c = 2$ (solid line) and 4 (dashed line) assisting nodes. For the random deployment strategy, $N_c = 2$ assisting nodes are considered.

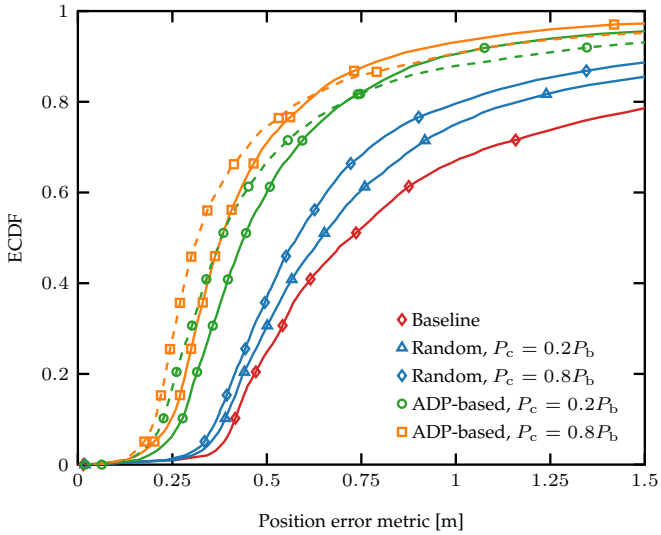

Fig. 9. ECDF of the position error metric for the ADP-based node deployment strategy with $P_c = 0.2P_b$ and $0.8P_b$, and $N_c = 2$ (solid line) and 4 (dashed line) assisting nodes in case C2. For the random deployment strategy, $N_c = 2$ assisting nodes are considered.

position error reductions of 67% and 69% for $M = 8$ and $M = 32$, respectively, over the baseline performance. While increasing M provides slight performance improvements, smaller values of M favor amenable complexity. Hence, deployment strategies with lower computational complexity can be implemented incurring in a small performance loss.

The impact of the transmitting power of assisting nodes on the localization performance is evaluated next. Fig. 8 shows the performance of the ADP-based strategy for deploying assisting nodes with $P_c = 0.2P_b$ and $0.8P_b$. The performance is evaluated for $N_c = 2$ and 4 assisting nodes with $M = 16$. The baseline performance and the random deployment strategy for $N_c = 2$ assisting nodes with $P_c = 0.2P_b$ and $0.8P_b$ are shown as benchmarks. Note that increasing the transmitting power of assisting nodes reduces the position error. Nonetheless, near-optimal node deployment strategies can provide adequate performance even with low transmitting resources (e.g., $P_c = 0.2P_b$). For example, the position errors using $N_c = 4$ assisting nodes with $P_c = 0.2P_b$ and $0.8P_b$ are below 0.45 m and below 0.34 m, respectively, for 90% of the cases. This corresponds to position error reductions of 62% and 70%, for $P_c = 0.2P_b$ and $P_c = 0.8P_b$, respectively, over the baseline performance. These results show that a near-optimal deployment of assisting nodes is beneficial for efficient localization.

Fig. 9 shows the performance of the ADP-based strategy for deploying assisting nodes with $P_c = 0.2P_b$ and $0.8P_b$, in case study C2. The performance is evaluated for $N_c = 2$ and 4 assisting nodes with $M = 16$. The baseline performance and the random deployment strategy for $N_c = 2$ assisting nodes with $P_c = 0.2P_b$ and $0.8P_b$ are shown as benchmarks. Note that the performance worsens compared to the scenario with the full anchor deployment due to the limited network infrastructure available (cf. Fig. 8). However, the proposed strategies also provide a significant performance improvement in this scenario. For example, the position errors for the baseline performance, and the random and ADP-based deployment strategies using $N_c = 2$ assisting nodes with $P_c = 0.2P_b$ are below 1.55 m, below 1.17 m, and below 0.71 m, respectively, for 80% of the cases. Here, the random and ADP-based deployment strategies reduce the position error by 24% and 54%, respectively, over the baseline performance. Hence, the developed strategies are also suitable for infrastructure-limited wireless environments.

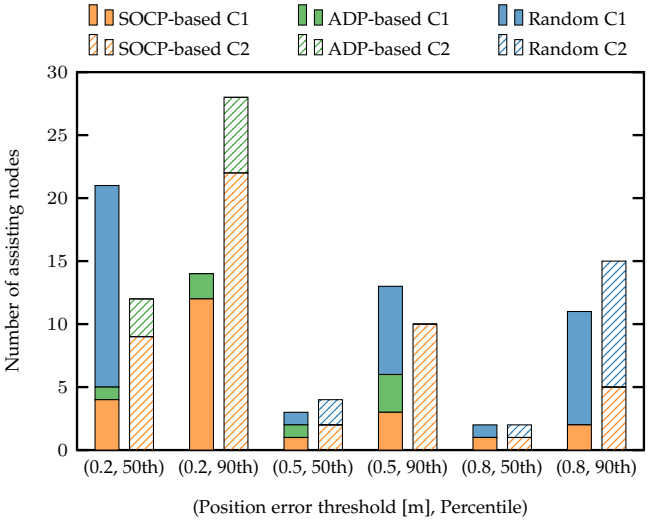

Fig. 10. Number of assisting nodes needed to meet given localization performance requirements using different node deployment strategies.

Next, consider the inverse node deployment problem of assisting nodes. Fig. 10 shows the number of assisting nodes needed to meet position error metrics, $\sqrt{\varrho}$, below 0.20, below 0.50, and below 0.80 m for 50% and 90% of the cases employing the SOCP-based, ADP-based, and random deployment strategies.[11] The strategies are evaluated with $M = 64$ and $P_c = 0.5P_b$ for both case studies C1 and C2. For the ADP-based strategy, the performance thresholds are set empirically to meet the requirements in terms of the

11. In particular, we consider the percentiles of the feasible instances of the problem.

position error metric with $\check{N} = 30$ assisting nodes. Such a value of $\check{N}$ is also considered to limit the number of assisting nodes in the random deployment strategy. In this figure, we consider only the number of assisting nodes for the SOCP-based strategy when it coincides with that for the ADP-based strategy. Similarly, the number of assisting nodes for the random deployment strategy is considered only when achieving the required performance is possible. For example, the random deployment strategy does not meet the requirement of position error below 0.20 m. Note that the developed near-optimal strategies reduce significantly the number of assisting nodes compared to the random deployment strategy. The number of assisting nodes increases as the performance requirements are more stringent either in terms of localization accuracy or percentage of cases. In case C2, the number of assisting nodes increases compared to case C1 due to the limited network infrastructure. The gaps between the SOCP- and ADP-based node deployment strategies are due to the use of different performance metrics. In particular, setting a threshold for the determinant of the EFIM for the position of the target agent is difficult because it cannot be related to a single localization error. Hence, employing the SPEB as performance metric for the inverse node deployment problem is more reasonable.

8 Conclusion

This paper presented near-optimal strategies to deploy assisting nodes for efficient network localization. Specifically, it introduced a methodology to determine a finite set of candidate positions and developed near-optimal strategies for deploying assisting nodes based on convex optimization and ADP for different problem formulations. A case study was presented to validate the proposed node deployment strategies and show the benefits of deploying assisting nodes in 3GPP scenarios. The results show that the developed near-optimal strategies provide a significant performance improvement and outperform the random deployment strategy. The amenable complexity of the ADP-based strategy makes it suitable for location-based services with stringent positioning latency requirements. Indeed, such a strategy aims to deploy assisting nodes with amenable complexity. The proposed strategies unleash the benefits of assisting nodes for accurate localization in complex and infrastructure-limited wireless environments.

Acknowledgments

The authors wish to thank R. Cohen and A. Vaccari for careful reading and helpful suggestions.

References

[1] M. Z. Win *et al.*, "Network localization and navigation via cooperation," *IEEE Commun. Mag.*, vol. 49, no. 5, pp. 56–62, May 2011.

[2] A. H. Sayed, A. Tarighat, and N. Khajehnouri, "Network-based wireless location: Challenges faced in developing techniques for accurate wireless location information," *IEEE Signal Process. Mag.*, vol. 22, no. 4, pp. 24–40, Jul. 2005.

[3] Y. Shen and M. Z. Win, "Fundamental limits of wideband localization – Part I: A general framework," *IEEE Trans. Inf. Theory*, vol. 56, no. 10, pp. 4956–4980, Oct. 2010.

[4] M. Chiani, A. Giorgetti, and E. Paolini, "Sensor radar for object tracking," *Proc. IEEE*, vol. 106, no. 6, pp. 1022–1041, Jun. 2018.

[5] X. Wang, L. Gao, and S. Mao, "CSI phase fingerprinting for indoor localization with a deep learning approach," *IEEE Internet of Things J.*, vol. 3, no. 6, pp. 1113–1123, Dec. 2016.

[6] X. Wang, X. Wang, and S. Mao, "Deep convolutional neural networks for indoor localization with CSI images," *IEEE Trans. Netw. Sci. Eng.*, vol. 7, no. 1, pp. 316–327, Jan.-Mar. 2020.

[7] X. Wang, L. Gao, and S. Mao, "BiLoc: Bi-modal deep learning for indoor localization with commodity 5GHz WiFi," *IEEE Access*, vol. 5, pp. 4209–4220, Mar. 2017.

[8] I. Dokmanić, R. Parhizkar, J. Ranieri, and M. Vetterli, "Euclidean distance matrices: Essential theory, algorithms, and applications," *IEEE Signal Process. Mag.*, vol. 32, no. 6, pp. 12–30, Nov. 2015.

[9] U. A. Khan, S. Kar, and J. M. F. Moura, "DILAND: An algorithm for distributed sensor localization with noisy distance measurements," *IEEE Trans. Signal Process.*, vol. 58, no. 3, pp. 1940–1947, Mar. 2010.

[10] U. Khan, S. Kar, and J. Moura, "Linear theory for self-localization: convexity, barycentric coordinates, and Cayley-Menger determinants," *IEEE Access*, vol. 3, pp. 1326 – 1339, Aug. 2015.

[11] S. Safavi, U. A. Khan, S. Kar, and J. M. F. Moura, "Distributed localization: A linear theory," *Proc. IEEE*, vol. 106, no. 7, pp. 1204–1223, Jul. 2018.

[12] A. Conti *et al.*, "Location awareness in beyond 5G networks," *IEEE Commun. Mag.*, vol. 59, no. 11, pp. 22–27, Nov. 2021, special issue on *Location Awareness for 5G and Beyond*.

[13] *Technical Specification Group Services and System Aspects; Service requirements for the 5G system; Stage 1*, 3rd Generation Partnership Project 3GPP™ TS 22.261 V18.3.0 (2021-06), Jun. 2021, Release 18.

[14] F. Morselli, S. M. Razavi, M. Z. Win, and A. Conti, "Soft information based localization for 5G networks and beyond," *IEEE Trans. Wireless Commun.*, vol. 22, pp. 1–16, 2023, to appear.

[15] J. Guivant, E. Nebot, and S. Baiker, "Autonomous navigation and map building using laser range sensors in outdoor applications," *J. of Robotic Systems*, vol. 17, no. 10, pp. 565–583, Oct. 2000.

[16] G. Zhan and W. Shi, "LOBOT: Low-cost, self-contained localization of small-sized ground robotic vehicles," *IEEE Trans. Parallel Distrib. Syst.*, vol. 24, no. 4, pp. 744–753, Apr. 2013.

[17] D. Wu, D. Chatzigeorgiou, K. Youcef-Toumi, and R. Ben-Mansour, "Node localization in robotic sensor networks for pipeline inspection," *IEEE Trans. Ind. Informat.*, vol. 12, no. 2, pp. 809–819, Apr. 2016.

[18] R. Karlsson and F. Gustafsson, "The future of automotive localization algorithms: Available, reliable, and scalable localization: Anywhere and anytime," *IEEE Signal Process. Mag.*, vol. 34, no. 2, pp. 60–69, Mar. 2017.

[19] J. Thomas, J. Welde, G. Loianno, K. Daniilidis, and V. Kumar, "Autonomous flight for detection, localization, and tracking of moving targets with a small quadrotor," *IEEE Robot. Autom. Lett.*, vol. 2, no. 3, pp. 1762–1769, Jul. 2017.

[20] F. Zabini and A. Conti, "Inhomogeneous Poisson sampling of finite-energy signals with uncertainties in $\mathbb{R}^d$," *IEEE Trans. Signal Process.*, vol. 64, no. 18, pp. 4679–4694, Sep. 2016.

[21] C. Jiang, L. Gao, L. Duan, and J. Huang, "Scalable mobile crowdsensing via peer-to-peer data sharing," *IEEE Trans. Mobile Comput.*, vol. 17, no. 4, pp. 898–912, Apr. 2018.

[22] S. Bartoletti, A. Conti, and M. Z. Win, "Device-free counting via wideband signals," *IEEE J. Sel. Areas Commun.*, vol. 35, no. 5, pp. 1163–1174, May 2017.

[23] T. Luo, S. S. Kanhere, J. Huang, S. K. Das, and F. Wu, "Sustainable incentives for mobile crowdsensing: Auctions, lotteries, and trust and reputation systems," *IEEE Commun. Mag.*, vol. 55, no. 3, pp. 68–74, Mar. 2017.

[24] T. Luo, J. Huang, S. S. Kanhere, J. Zhang, and S. K. Das, "Improving IoT data quality in mobile crowd sensing: A cross validation approach," *IEEE Internet of Things J.*, vol. 6, no. 3, pp. 5651–5664, Jun. 2019.

[25] Z. Liu, A. Conti, S. K. Mitter, and M. Z. Win, "Communication-efficient distributed learning over networks–Part I: Sufficient conditions for accuracy," *IEEE J. Sel. Areas Commun.*, vol. 41, no. 4, pp. 1081–1101, Apr. 2023, special issue on *Communication-Efficient Distributed Learning Over Networks*.

[26] Z. Liu, A. Conti, S. K. Mitter, and M. Z. Win, "Communication-efficient distributed learning over networks–Part II: Necessary conditions for accuracy," *IEEE J. Sel. Areas Commun.*, vol. 41, no. 4,

pp. 1102–1119, Apr. 2023, special issue on *Communication-Efficient Distributed Learning Over Networks*.

[27] G. Cardone *et al.*, "Fostering participaction in smart cities: a geo-social crowdsensing platform," *IEEE Commun. Mag.*, vol. 51, no. 6, pp. 112–119, Jun. 2013.

[28] A. Zanella, N. Bui, A. Castellani, L. Vangelista, and M. Zorzi, "Internet of Things for smart cities," *IEEE Internet Things J.*, vol. 1, no. 1, pp. 22–32, Feb. 2014.

[29] M. Z. Win, Z. Wang, Z. Liu, Y. Shen, and A. Conti, "Location awareness via intelligent surfaces: A path toward holographic NLN," *IEEE Veh. Technol. Mag.*, vol. 17, no. 2, pp. 37–45, Jun. 2022, special issue on *Backscatter and Reconfigurable Intelligent Surface Empowered Wireless Communications in 6G*.

[30] V. Moreno, M. A. Zamora, and A. F. Skarmeta, "A low-cost indoor localization system for energy sustainability in smart buildings," *IEEE Sensors J.*, vol. 16, no. 9, pp. 3246–3262, May 2016.

[31] Z. Wang, Z. Liu, Y. Shen, A. Conti, and M. Z. Win, "Location awareness in beyond 5G networks via reconfigurable intelligent surfaces," *IEEE J. Sel. Areas Commun.*, vol. 40, no. 7, pp. 2011–2025, Jul. 2022, special issue on *Integrated Sensing and Communication*.

[32] K. Lin, M. Chen, J. Deng, M. M. Hassan, and G. Fortino, "Enhanced fingerprinting and trajectory prediction for IoT localization in smart buildings," *IEEE Trans. Autom. Sci. Eng.*, vol. 13, no. 3, pp. 1294–1307, Jul. 2016.

[33] G. Pasolini *et al.*, "Smart city pilot projects using LoRa and IEEE 802.15.4 technologies," *MDPI Sensors*, vol. 18, no. 4, Apr. 2018.

[34] A. Conti, S. Mazuelas, S. Bartoletti, W. C. Lindsey, and M. Z. Win, "Soft information for localization-of-things," *Proc. IEEE*, vol. 107, no. 11, pp. 2240–2264, Nov. 2019.

[35] D. Zhang, L. T. Yang, M. Chen, S. Zhao, M. Guo, and Y. Zhang, "Real-time locating systems using active RFID for Internet of Things," *IEEE Syst. J.*, vol. 10, no. 3, pp. 1226–1235, Sep. 2016.

[36] M. Z. Win, F. Meyer, Z. Liu, W. Dai, S. Bartoletti, and A. Conti, "Efficient multi-sensor localization for the Internet of Things," *IEEE Signal Process. Mag.*, vol. 35, no. 5, pp. 153–167, Sep. 2018.

[37] N. C. Luong, D. T. Hoang, P. Wang, D. Niyato, D. I. Kim, and Z. Han, "Data collection and wireless communication in Internet of Things (IoT) using economic analysis and pricing models: A survey," *IEEE Commun. Surveys Tuts.*, vol. 18, no. 4, pp. 2546–2590, 2016.

[38] S. G. Nagarajan, P. Zhang, and I. Nevat, "Geo-spatial location estimation for Internet of Things (IoT) networks with one-way time-of-arrival via stochastic censoring," *IEEE Internet Things J.*, vol. 4, no. 1, pp. 205–214, Feb. 2017.

[39] *Technical Specification Group Services and System Aspects; Service requirements for cyber-physical control applications in vertical domains; Stage 1*, 3rd Generation Partnership Project 3GPP™ TS 22.104 V18.3.0 (2021-12), Dec. 2021, Release 18.

[40] *Technical Specification Group Services and System Aspects; Study on positioning use cases; Stage 1*, 3rd Generation Partnership Project 3GPP™ TR 22.872 V16.1.0 (2018-09), Sep. 2018, Release 16.

[41] M. Z. Win, W. Dai, Y. Shen, G. Chrisikos, and H. V. Poor, "Network operation strategies for efficient localization and navigation," *Proc. IEEE*, vol. 106, no. 7, pp. 1224–1254, Jul. 2018, special issue on *Foundations and Trends in Localization Technologies*.

[42] G. Torsoli, M. Z. Win, and A. Conti, "Blockage intelligence in complex environments for beyond 5G localization," *IEEE J. Sel. Areas Commun.*, vol. 41, no. 6, pp. 1688–1701, Jun. 2023, special issue on *3GPP Technologies: 5G-Advanced and Beyond*.

[43] E. Maşazade, R. Niu, P. K. Varshney, and M. Keskinoz, "Energy aware iterative source localization for wireless sensor networks," *IEEE Trans. Signal Process.*, vol. 58, no. 9, pp. 4824–4835, Jun. 2010.

[44] Y. Shen, W. Dai, and M. Z. Win, "Power optimization for network localization," *IEEE/ACM Trans. Netw.*, vol. 22, no. 4, pp. 1337–1350, Aug. 2014.

[45] H. Godrich, A. P. Petropulu, and H. V. Poor, "Power allocation strategies for target localization in distributed multiple-radar architectures," *IEEE Trans. Signal Process.*, vol. 59, no. 7, pp. 3226–3240, Jul. 2011.

[46] T. Wang, Y. Shen, A. Conti, and M. Z. Win, "Network navigation with scheduling: Error evolution," *IEEE Trans. Inf. Theory*, vol. 63, no. 11, pp. 7509–7534, Nov. 2017.

[47] S. Dwivedi, D. Zachariah, A. De Angelis, and P. Händel, "Cooperative decentralized localization using scheduled wireless transmissions," *IEEE Commun. Lett.*, vol. 17, no. 6, pp. 1240–1243, Jun. 2013.

[48] T. Wang, A. Conti, and M. Z. Win, "Network navigation with scheduling: Distributed algorithms," *IEEE/ACM Trans. Netw.*, vol. 27, no. 4, pp. 1319–1329, Aug. 2019.

[49] C. A. Gómez-Vega, Z. Liu, C. A. Gutiérrez, A. Conti, and M. Z. Win, "Network localization with assisting nodes," in *Proc. The Korean Inst. of Commun. and Inf. Sciences Winter Conf.*, Pyeongchang, Korea, Feb. 2021, pp. 269–272.

[50] C. Fan, C. She, H. Zhang, B. Li, C. Zhao, and D. Niyato, "Learning to optimize user association and spectrum allocation with partial observation in mmWave-enabled UAV networks," *IEEE Trans. Wireless Commun.*, vol. 21, no. 8, pp. 5873–5888, Aug. 2022.

[51] X. Pang, N. Zhao, J. Tang, C. Wu, D. Niyato, and K.-K. Wong, "IRS-assisted secure UAV transmission via joint trajectory and beamforming design," *IEEE Trans. Commun.*, vol. 70, no. 2, pp. 1140–1152, Feb. 2022.

[52] X. Pang, M. Sheng, N. Zhao, J. Tang, D. Niyato, and K.-K. Wong, "When UAV meets IRS: Expanding air-ground networks via passive reflection," *IEEE Wireless Commun.*, vol. 28, no. 5, pp. 164–170, Oct. 2021.

[53] A. Conti, M. Guerra, D. Dardari, N. Decarli, and M. Z. Win, "Network experimentation for cooperative localization," *IEEE J. Sel. Areas Commun.*, vol. 30, no. 2, pp. 467–475, Feb. 2012.

[54] Z. Liu, W. Dai, and M. Z. Win, "Mercury: An infrastructure-free system for network localization and navigation," *IEEE Trans. Mobile Comput.*, vol. 17, no. 5, pp. 1119–1133, May 2018.

[55] B. Teague, Z. Liu, F. Meyer, A. Conti, and M. Z. Win, "Network localization and navigation with scalable inference and efficient operation," *IEEE Trans. Mobile Comput.*, vol. 21, no. 6, pp. 2072–2087, Jun. 2022.

[56] E. Amaldi, A. Capone, and F. Malucelli, "Planning UMTS base station location: Optimization models with power control and algorithms," *IEEE Trans. Wireless Commun.*, vol. 2, no. 5, pp. 939–952, Sep. 2003.

[57] J. Guo and H. Jafarkhani, "Sensor deployment with limited communication range in homogeneous and heterogeneous wireless sensor networks," *IEEE Trans. Wireless Commun.*, vol. 15, no. 10, pp. 6771–6784, Oct. 2016.

[58] M. Mozaffari, W. Saad, M. Bennis, and M. Debbah, "Efficient deployment of multiple unmanned aerial vehicles for optimal wireless coverage," *IEEE Commun. Lett.*, vol. 20, no. 8, pp. 1647–1650, Aug. 2016.

[59] M. Laghate and D. Cabric, "Learning wireless networks' topologies using asymmetric Granger causality," *IEEE J. Sel. Topics Signal Process.*, vol. 12, no. 1, pp. 233–247, Feb. 2018.

[60] S. Hanna, E. Krijestorac, and D. Cabric, "UAV swarm position optimization for high capacity MIMO backhaul," *IEEE J. Sel. Areas Commun.*, vol. 39, no. 10, pp. 3006–3021, Oct. 2021.

[61] S. Hanna, H. Yan, and D. Cabric, "Distributed UAV placement optimization for cooperative line-of-sight MIMO communications," in *Proc. IEEE Int. Conf. Acoustics, Speech, and Signal Process.*, Brighton, UK, 2019, pp. 4619–4623.

[62] Z. Gao, D. Chen, S. Cai, and H.-C. Wu, "OptDynLim: An optimal algorithm for the one-dimensional RSU deployment problem with nonuniform profit density," *IEEE Trans. Ind. Informat.*, vol. 15, no. 2, pp. 1052–1061, Feb. 2019.

[63] Z. Gao, D. Chen, S. Cai, and H.-C. Wu, "Optimal and greedy algorithms for the one-dimensional RSU deployment problem with new model," *IEEE Trans. Veh. Technol.*, vol. 67, no. 8, pp. 7643–7657, Aug. 2018.

[64] Z. Gao, H.-C. Wu, S. Cai, and G. Tan, "Tight approximation ratios of two greedy algorithms for optimal RSU deployment in one-dimensional VANETs," *IEEE Trans. Veh. Technol.*, vol. 70, no. 1, pp. 3–17, Jan. 2021.

[65] J. N. Ash and R. L. Moses, "On optimal anchor node placement in sensor localization by optimization of subspace principal angles," in *Proc. IEEE Int. Conf. Acoustics, Speech, and Signal Process.*, Las Vegas, NV, Mar. 2008, pp. 2289–2292.

[66] A. N. Bishop, B. Fidan, B. D. Anderson, K. Doğançay, and P. N. Pathirana, "Optimality analysis of sensor-target localization geometries," *Automatica*, vol. 46, no. 3, pp. 479–492, Mar. 2010.

[67] W. Suwansantisuk and H. Lu, "Localization in the unknown environments and the principle of anchor placement," in *Proc. IEEE Int. Conf. Commun.*, London, UK, Jun. 2015, pp. 2488–2494.

[68] W. Shi *et al.*, "Simple solution to the optimal deployment of cooperative nodes in two-dimensional TOA-based and AOA-based localization system," *EURASIP J. Wireless Commun. and Netw.*, vol. 2017, pp. 1–16, Dec. 2017.

[69] H. Chen, Q. Shi, P. Huang, H. V. Poor, and K. Sezaki, "Mobile anchor assisted node localization for wireless sensor networks," in *Proc. IEEE Int. Symp. on Personal, Indoor and Mobile Radio Commun.*, Tokyo, Japan, Sep. 2009, pp. 87–91.

[70] S. Martínez and F. Bullo, "Optimal sensor placement and motion coordination for target tracking," *Automatica*, vol. 42, no. 4, pp. 661–668, Apr. 2006.

[71] D. B. Jourdan and N. Roy, "Optimal sensor placement for agent localization," *ACM Transactions on Sensor Networks*, vol. 4, no. 3, pp. 13:1–40, May 2008.

[72] M. Posluk, J. Ahlander, D. Shrestha, S. M. Razavi, G. Lindmark, and F. Gunnarsson, "5G deployment strategies for high positioning accuracy in indoor environments," in *Proc. Int. Conf. Indoor Positioning and Indoor Navigation WiP*, Lloret de Mar, Spain, Nov. 2021, pp. 1–15.

[73] W. Zhao, A. Goudar, and A. P. Schoellig, "Finding the right place: Sensor placement for UWB time difference of arrival localization in cluttered indoor environments," *IEEE Robot. Autom. Lett.*, vol. 7, no. 3, pp. 6075–6082, Jul. 2022.

[74] J. J. Khalife and Z. M. Kassas, "Optimal sensor placement for dilution of precision minimization via quadratically constrained fractional programming," *IEEE Trans. Aerosp. Electron. Syst.*, vol. 55, no. 4, pp. 2086–2096, Aug. 2019.

[75] H. L. Van Trees, K. L. Bell, and Z. Tian, *Detection, Estimation, and Modulation Theory, Part I: Detection, Estimation, and Filtering Theory*, 2nd ed. New York, NY: John Wiley & Sons, Inc., 2013.

[76] M. Z. Win, Y. Shen, and W. Dai, "A theoretical foundation of network localization and navigation," *Proc. IEEE*, vol. 106, no. 7, pp. 1136–1165, Jul. 2018, special issue on *Foundations and Trends in Localization Technologies*.

[77] S. Joshi and S. Boyd, "Sensor selection via convex optimization," *IEEE Trans. Signal Process.*, vol. 57, no. 2, pp. 451–462, Feb. 2009.

[78] E. Masazade, R. Niu, and P. K. Varshney, "Dynamic bit allocation for object tracking in wireless sensor networks," *IEEE Trans. Signal Process.*, vol. 60, no. 10, pp. 5048–5063, Oct. 2012.

[79] D. P. Bertsekas, *Nonlinear Programming*, 3rd ed. Belmont, MA: Athena Scientific, 2016.

[80] S. Boyd and L. Vandenberghe, *Convex Optimization*. Cambridge, UK: Cambridge University Press, 2004.

[81] *Technical Specification Group Radio Access Network; Study on scenarios and requirements of in-coverage, partial coverage, and out-of-coverage NR positioning use cases*, 3rd Generation Partnership Project 3GPP™ TR 38.845 V17.0.0 (2021-09), Sep. 2021, Release 17.

[82] *Technical Specification Group Services and System Aspects; Study on architecture enhancement to support ranging based services and sidelink positioning*, 3rd Generation Partnership Project 3GPP™ TR 23.700-86 V1.2.0 (2022-11), Nov. 2022, Release 18.

[83] *Technical Specification Group Radio Access Network; Study on expanded and improved NR positioning*, 3rd Generation Partnership Project 3GPP™ TR 38.859 V18.0.0 (2022-12), Dec. 2022, Release 18.

[84] I. Rahman *et al.*, "5G evolution toward 5G Advanced: An overview of 3GPP releases 17 and 18," *Ericsson Technol. Rev.*, vol. 105, no. 1, pp. 56–66, Apr. 2022.

[85] C. A. Gómez-Vega, F. Morselli, M. Z. Win, and A. Conti, "A statistical range information model with application to UWB localization," in *Proc. Military Commun. Conf.*, San Diego, CA, Nov. 2021, pp. 538–543.

[86] M. Grant and S. Boyd, "CVX: Matlab software for disciplined convex programming, version 2.2," http://cvxr.com/cvx, Jan. 2020.

[87] M. S. Lobo, L. Vandenberghe, S. Boyd, and H. Lebret, "Applications of second-order cone programming," *Linear Algebra and its Applications*, vol. 284, no. 1-3, pp. 193–228, Nov. 1998.

[88] D. P. Bertsekas, *Dynamic Programming and Optimal Control, volume I*, 4th ed. Belmont, MA: Athena Scientific, 2017.

[89] D. P. Bertsekas, *Reinforcement Learning and Optimal Control*, 1st ed. Belmont, MA: Athena Scientific, 2019.

[90] D. P. Bertsekas, *Rollout, Policy Iteration, and Distributed Reinforcement Learning*. Belmont, MA: Athena Scientific, 2020.

[91] J. Ding and A. Zhou, "Eigenvalues of rank-one updated matrices with some applications," *Appl. Math. Lett.*, vol. 20, no. 12, pp. 1223–1226, Dec. 2007.

[92] M. Z. Win and R. A. Scholtz, "Ultra-wide bandwidth time-hopping spread-spectrum impulse radio for wireless multiple-access communications," *IEEE Trans. Commun.*, vol. 48, no. 4, pp. 679–691, Apr. 2000.

[93] M. Z. Win and R. A. Scholtz, "Impulse radio: How it works," *IEEE Commun. Lett.*, vol. 2, no. 2, pp. 36–38, Feb. 1998.

[94] M. Z. Win and R. A. Scholtz, "On the robustness of ultra-wide bandwidth signals in dense multipath environments," *IEEE Commun. Lett.*, vol. 2, no. 2, pp. 51–53, Feb. 1998.

[95] M. Z. Win, "Spectral density of random UWB signals," *IEEE Commun. Lett.*, vol. 6, no. 12, pp. 526–528, Dec. 2002.

[96] S. Gezici *et al.*, "Localization via ultra-wideband radios: A look at positioning aspects for future sensor networks," *IEEE Signal Process. Mag.*, vol. 22, no. 4, pp. 70–84, Jul. 2005.

[97] 5G-PPP Architecture Working Group, *View on 5G Architecture*. The 5G Infrastructure Public Private Partnership, Aug. 2021, version 4.0.

[98] *Technical Specification Group Radio Access Network; Study on channel model for frequencies from 0.5 to 100 GHz*, 3rd Generation Partnership Project 3GPP™ 3GPP TR 38.901 V16.1.0 (2019-12), Dec. 2019, Release 16.

[99] "IEEE standard for information technology - telecommunications and information exchange between systems - local and metropolitan area networks - specific requirement part 15.4: Wireless medium access control (MAC) and physical layer (PHY) specifications for low-rate wireless personal area networks (WPANs)," *IEEE Std 802.15.4a-2007 (Amendment to IEEE Std 802.15.4-2006)*, pp. 1–203, 2007.

[100] A. F. Molisch *et al.*, "A comprehensive standardized model for ultrawideband propagation channels," *IEEE Trans. Antennas Propag.*, vol. 54, no. 11, pp. 3151–3166, Nov. 2006, special issue on *Wireless Communications*.

[101] F. Ademaj, M. K. Müller, S. Schwarz, and M. Rupp, "Modeling of spatially correlated geometry-based stochastic channels," in *Proc. IEEE Semiannual Veh. Technol. Conf.*, Toronto, Canada, Sep. 2017.

[102] F. Ademaj, S. Schwarz, T. Berisha, and M. Rupp, "A spatial consistency model for geometry-based stochastic channels," *IEEE Access*, vol. 7, pp. 183 414–183 427, 2019.

Carlos A. Gómez-Vega (Graduate Student Member, IEEE) received the M.S. degree in electronic engineering from the Universidad Autónoma de San Luis Potosí, San Luis Potosí, Mexico, in 2020. He is currently pursuing the Ph.D. degree with the Wireless Communication and Localization Networks Laboratory, University of Ferrara, Italy.

Since 2020, he has been a Research Assistant with the Wireless Communication and Localization Networks Laboratory, University of Ferrara. In 2019, he was a Visiting Student with the Wireless Information and Network Sciences Laboratory, Massachusetts Institute of Technology, USA. His current research interests include network localization and navigation, and wireless resource optimization.

Mr. Gómez-Vega received the Best Paper Award from the IEEE LATINCOM in 2019. He also serves as a reviewer for various IEEE journals and international conferences.

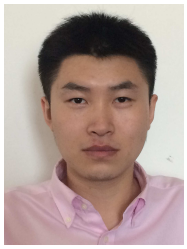

Zhenyu Liu (Member, IEEE) received the B.S. degree (with honor) and M.S. degrees in electronic engineering from Tsinghua University, Beijing, China, in 2011 and 2014, respectively, and the S.M. degree in aeronautics and astronautics and Ph.D. degree in networks and statistics from the Massachusetts Institute of Technology (MIT) in 2022.

Since 2022, he has been a Post-Doctoral Associate in the wireless information and network sciences laboratory at MIT. His research interests include wireless communications, network localization, distributed inference, networked control, and quantum information science.

Dr. Liu received the first prize of the IEEE Communications Society's Student Competition in 2016 and 2019, the R&D100 Award for Peregrine System in 2018, and the Best Paper Award at the IEEE Latin-American Conference on Communications in 2017.

Carlos A. Gutiérrez (Senior Member, IEEE) received the B.E. degree in electronics and digital communication systems from the Universidad Autónoma de Aguascalientes, Mexico, in 2002, the Advanced Studies Diploma degree in signal processing and communication theory from the Universidad Politécnica de Cataluña, Spain, in 2005, the M.S. degree in electronics and telecommunications from CICESE, Mexico, in 2006, and the Ph.D. degree in mobile communication systems from the University of Agder, Norway, in 2009.

From 2009 to 2011, he was with the School of Engineering, Universidad Panamericana, Aguascalientes, Mexico. Since January 2012, he has been with the Faculty of Science, Universidad Autónoma de San Luis Potosí, Mexico. His research interests include modeling, simulation, and measurement of wireless channels; antenna design; vehicular communications; and wireless perception systems for human activity recognition.

Dr. Gutiérrez is a member of the Technical Committee on Propagation of the IEEE Vehicular Technology Society. His publications received three best paper awards. He has held different positions in organizing and technical program committees of various international conferences. He has served as an Expert Evaluator for the European Commission and CONACYT (Mexico); an associate editor for the *IEEE Vehicular Technology Magazine*; and a guest editor for international journals.

Moe Z. Win (Fellow, IEEE) is a Professor at the Massachusetts Institute of Technology (MIT) and the founding director of the Wireless Information and Network Sciences Laboratory. Prior to joining MIT, he was with AT&T Research Laboratories and with NASA Jet Propulsion Laboratory.

His research encompasses fundamental theories, algorithm design, and network experimentation for a broad range of real-world problems. His current research topics include ultra-wideband systems, network localization and navigation, network interference exploitation, and quantum information science. He has served the IEEE Communications Society as an elected Member-at-Large on the Board of Governors, as elected Chair of the Radio Communications Committee, and as an IEEE Distinguished Lecturer. Over the last two decades, he held various editorial positions for IEEE journals and organized numerous international conferences. Recently, he has served on the SIAM Diversity Advisory Committee.

Dr. Win is an elected Fellow of the AAAS, the EURASIP, the IEEE, and the IET. He was honored with two IEEE Technical Field Awards: the IEEE Kiyo Tomiyasu Award (2011) and the IEEE Eric E. Sumner Award (2006, jointly with R. A. Scholtz). His publications, co-authored with students and colleagues, have received several awards. Other recognitions include the MIT Everett Moore Baker Award (2022), the IEEE Vehicular Technology Society James Evans Avant Garde Award (2022), the IEEE Communications Society Edwin H. Armstrong Achievement Award (2016), the Cristoforo Colombo International Prize for Communications (2013), the Copernicus Fellowship (2011) and the *Laurea Honoris Causa* (2008) from the Università degli Studi di Ferrara, and the U.S. Presidential Early Career Award for Scientists and Engineers (2004). He is an ISI Highly Cited Researcher.

Andrea Conti (Fellow, IEEE) is a Professor and founding director of the Wireless Communication and Localization Networks Laboratory at the University of Ferrara, Italy. Prior to joining the University of Ferrara, he was with CNIT and with IEIIT-CNR.

In Summer 2001, he was with the Wireless Systems Research Department at AT&T Research Laboratories. Since 2003, he has been a frequent visitor to the Wireless Information and Network Sciences Laboratory at the Massachusetts Institute of Technology, where he presently holds the Research Affiliate appointment. His research interests involve theory and experimentation of wireless communication and localization systems. His current research topics include network localization and navigation, distributed sensing, adaptive diversity communications, and quantum information science.

Dr. Conti has served as editor for IEEE journals and chaired international conferences. He was elected Chair of the IEEE Communications Society's Radio Communications Technical Committee and is Co-founder of the IEEE Quantum Communications & Information Technology Emerging Technical Subcommittee. He received the HTE Puskás Tivadar Medal, the IEEE Communications Society's Fred W. Ellersick Prize, and the IEEE Communications Society's Stephen O. Rice Prize in the field of Communications Theory. He is an elected Fellow of the IEEE and of the IET, and a member of Sigma Xi. He has been selected as an IEEE Distinguished Lecturer.